SIMULATION OF FLOW OVER A GAS TURBINE COMPRESSOR BLADE RUNNING ON AIR AND SYNGAS

LIZ WANGUI MAINA

MASTER OF SCIENCE

(Mechanical Engineering)

JOMO KENYATTA UNIVERSITY OF AGRICULTURE AND TECHNOLOGY

2022

Simulation of Flow Over of a Gas Turbine Compressor Blade Running on Air and Syngas

Liz Wangui Maina

A Thesis Submitted in Partial Fulfillment of the Requirements for the Degree of Master of Science in Mechanical Engineering of the Jomo Kenyatta University of Agriculture and Technology

2022

DECLARATION

This thesis is my original work and has not been presented for a degree in this or any other university.

Signature:..... Date...../...../.....

Liz Wangui Maina

This thesis has been submitted for examination with our approval as the university supervisors.

Signature:..... Date...../...../.....

Dr.(Eng.) Hiram M. Ndiritu, PhD.

JKUAT, Kenya

Signature:..... Date...../...../.....

Dr. Benson B. Gathitu, PhD.

JKUAT, Kenya

DEDICATION

I dedicate this work to the Almighty God and to my loving, and patient family. To my family for all their encouragement this far. The journey was challenging but with your prayers, and encouragement I managed and pulled through.

ACKNOWLEDGMENT

To God be the glory for by His strength, and abounding love, I have been able to reach this far. My sincere appreciation goes to my supervisors, Dr.(Eng) H. Ndiritu and Dr. B. Gathitu for their endless guidance, support, patience and encouragement during my research. I would also like to thank the Government of Kenya through JKUAT for giving me a scholarship to do Msc. Mechanical Engineering.

I would want to extend my gratitude to the staff, technicians and technologist of the department of Mechanical Engineering, and the post graduate students for their support. They were present during the presentations and their questions helped me streamline my work.

TABLE OF CONTENTS

LIST OF TABLES

LIST OF FIGURES

LIST OF ABBREVIATIONS

ANSYS	Analysis System
CAD	Computer Aided Design
CATIA	Computer Aided Three-dimensional Interactive Application
FEA	Finite Element Analysis
GDP	Gross Domestic Product
IGES	Initial Graphics Exchange Specification
IGCC	Integrated Gasification Combined Cycle
KNBS	Kenya National Bureau of Statistics
ICE	Internal Combustion Engine
TPM	Total Particulate Matter
LES	Large Eddy Simulation
RPM	Revolutions Per Minute
GDP	Gross Domestic Product
ANSYS	Analysis of System
GHG	Green House Gases
PM	Particulate Matter
CO_2	Carbon Dioxide
GE	General Electric
HFO	Heavy Fuel Oil
CO	Carbon Monoxide
H_2	Hydrogen Gas
kWh	kiloWatt-hour
CH_4	Methane
MW	Mega Watt

LIST OF NOTATIONS

C	Specific heat capacity, in kJ/kgK
T	Temperature, in Kelvin
p	Pressure, in Pascal
m	Mass, in kilogrammes
x	Thickness, in metres
d	Diameter, in metres
l	Length, in metres
t	Time, in seconds
W	Watt

LIST OF SYMBOLS

∂	Partial differentiation
ω	Turbulence Frequency
μ	Viscosity Coefficient
$\mathbf{k}$	Turbulent Kinetic Energy
∇	Divergence
ρ	Density
$\mathbf{V}$	Velocity Vector

ABSTRACT

There has been an increase in demand for electricity globally. Gas turbines running on syngas are being used to generate electricity. This is because syngas is a renewable source of energy. As of 1999, General Electric (GE) had twelve gas turbines in operation using syngas in Delaware and Singapore. Though gas turbines using syngas are in use, there is little literature showing the performance of the compressors in the gas turbines and specifically centrifugal compressors. This research focused on the performance of a centrifugal compressor running on syngas and compared its performance with that running on air. The syngas used was a mixture of carbon monoxide (CO) and hydrogen (H_2). The centrifugal compressor designed was unshrouded with 15 main blades at a backsweep angle of 45^0 and a vaneless diffuser. An initial rotational speed of 22,000 RPM was input with a mass flowrate 0.167 kg/s for air. An inlet pressure and temperature of 1 bar and 298 K respectively were also input. These values were obtained from literature. Total heat transfer was chosen and turbulence model used was shear stress transport. The results showed that at low mass flow rates and high rotational speed, air as a medium generated recirculation regions as compared to syngas. The centrifugal compressor using air had recirculation regions from 20% span all the way to 80% span while for syngas the recirculation was at 80% span. Air velocity reached a maximum of 50 m/s for air and 140 m/s for syngas. For syngas, the pressure contours showed a decrease in pressure through the meridional passage while for air, there was a pressure increase. This research can be applied to industries working with syngas gas turbines for power generation, and compressing syngas for domestic use. Research can be further streamlined to focus on using syngas as a fuel for automobiles.

CHAPTER ONE

INTRODUCTION

1.1 BACKGROUND

Electricity is the fastest growing form of end use energy consumption ("International Energy Outlook May 2016", n.d.). Fossil fuels and coal have been used to produce electricity in most countries. Energy demand has been growing rapidly because of an increase in population, industries and the need to improve living standards. In the last two decades, electricity production has risen by 76% (Council, 2013). This has led to an increase in use of coal by 68%, natural gas by 62%, oil by 25%, hydropower by 21%, and nuclear energy by 13% from 2006 to 2016.

Kenya relies on hydro-power, geothermal,and thermal power as the main source of electricity generation ("Kenya National Bureau of Statistics: Statistical Abstract 2015", n.d.). The fluctuation of the hydro power is caused by fluctuating river flow in particular Tana river which is the source of the 7-Folk dam, extreme evaporation rates, and sedimentation and siltation in the dams (Bunyasi, 2012). Figure 1.1 shows annual comparison of hydro, thermal and geothermal electricity power generation from 2006 to 2014. This evidently shows that hydro remains the greatest source of power in Kenya.

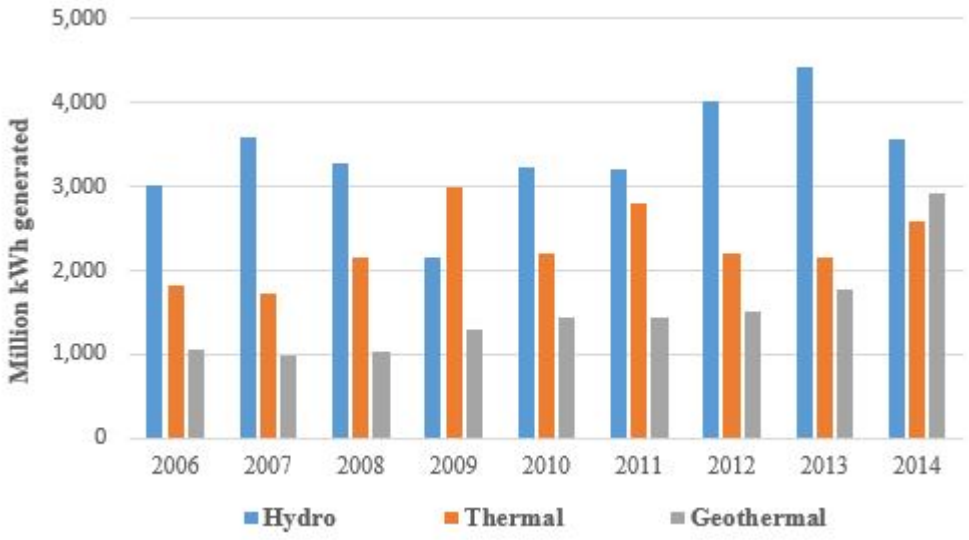

Figure 1.1: Electricity Generated in Kenya from 2006-2014 ("Kenya National Bureau of Statistics: Statistical Abstract 2015", n.d.)

Government has embarked on exploiting other energy sources of energy such as geothermal, wind, solar and coal to supplement hydro power in meeting electricity demand.

In KenGen's 2017 annual report (*KenGen's INTEGRATED ANNUAL REPORT & FINANCIAL STATEMENTS FOR THE YEAR ENDED 30 JUNE 2017*, 2017), thermal energy accounted for 16% of the electricity capacity mix. This translates to over 250 MW of installed thermal capacity. Thermal energy is from both diesel and gas turbine engines. The diesel engines run on Heavy Fuel Oil (HFO) while the gas turbines run on kerosene. The gas turbines are installed in Embakasi and Muhoroni and they have an installation capacity of about 60 MW(*KenGen's INTEGRATED ANNUAL REPORT & FINANCIAL STATEMENTS FOR THE YEAR ENDED 30 JUNE 2017*, 2017).

Gas turbine design comprises of a compressor, a combustor, and a turbine. A compressor is utilized in raising the pressure of the fluid before combustion while the turbine expands it. Some of the problems facing gas turbines in their operations

are overheating turbine blades; choke, surge, and stall in the compressor as well as degradation of blades due to wear(Burnes, 2018).

Implementation of coal projects to produce electric power is hampered by negative effect on environmental and health caused by run-of-mine coal combustion. When coal is burned in its raw form, it emits green house gases such as CO_2 (carbon dioxide),CO (carbon monoxide) , CH_4 (methane) , mercury and other toxic gases to the atmosphere. When underground coal is exposed to the atmosphere, the sulphur in the pyrite reacts with oxygen to form sulphate, and in the presence of water it forms sulphuric acid. The sulphuric acid formed is drained off to water channels resulting in contamination of the water (*Emissions from Coal Fires and Their Impact on the Environment*, 2009). On the other hand, smoke resulting from burning of coal causes asthma, and other respiratory problems (Zhang, 2014).

One of the ways of utilizing coal while reducing its emissions is through Integrated Gasification Combined Cycle (IGCC) and coal gasification. In India, coal emission is reduced through underground coal gasification(Khadse, 2007) , and also by cleaning using leaching reagent(Barma, n.d.). Discovery and subsequent mining of coal at Mui basin in Kenya is expected to boost electric power generation and supply. The electricity from coal is also expected to reduce importation of electricity from neighbouring countries, Uganda and Tanzania. Meanwhile, it is essential to identify clean coal utilization mechanisms that ensure power generation from coal fuel is conducted in a sustainable and clean manner. One way of such mechanisms is gasification which results in formation of syngas.

1.2 SYNGAS UTILIZATION IN POWER GENERATION

The use of syngas energy is one way of generating clean energy from coal. Syngas is obtained from coal, biomass or solid waste through gasification processes. Gasifica-

tion involves burning materials that have carbon in limited supply of oxygen(Chen, 2015). A feature of syngas is that, unlike the raw fuels it is derived from, it can be utilized in gas turbine systems to produce electric power (Nucara, 2013). Gas turbine systems are more compact, their mechanical efficiency is higher, and they can be started and stopped more quickly than other Internal Combustion Engines (ICE) (Oyedepo, 2014). Syngas can also be fed into a solid oxide fuel cell to generate electricity. A solid oxide fuel cell is an energy conversion device that produces electricity from oxidizing a fuel(Chen, 2015). Coal from Mui basin in Kenya can be gasified and the syngas produced used to run a gas turbine coupled to a generator therefore producing electricity.

1.3 PROBLEM STATEMENT

Globally, energy demand has been on the rise due to economic development of countries, improved living standards, and industrialization. In Kenya, the need for energy has been on the rise. In 2019, Kenya had an installed capacity of 828 MW of geothermal energy, 826 MW of hydro power,749 MW of thermal power and 331 MW of wind power (*USAID Kenya: Power Africa Fact Sheet*, n.d.). The frequency of power outages is high (33% compared with the average for Mexico, China and South Africa, which stands at 1%). Production lost due to these outages is approximately 9.3% (compared with the average for Mexico, China and South Africa, which stands at 1.8%).

The emission of carbon dioxide from existing coal based power plants is however considered as one of the main factors responsible for climate change, due to its severe greenhouse effect(Rubanova, n.d.). CO_2 (Carbon dioxide), sulphur and Total Particulate Matter (TPM) produced during coal combustion led to build up of smog, haze, and acid rain in China. Most of the population in China has been exposed

to PM 2.5 which are tiny particles that penetrate into the lungs and cause asthma, lung cancer and heart problems(Zhang, 2014).

Though gas turbines are compact and have high efficiencies, they are not the most used Internal Combustion Engines (ICE) for power generation. Gas turbines components particularly compressors experience several problems some of which are stage matching, large tip clearances of blade, eccentricity and service life degradation blade failures caused by frequent surge-induced fatigue(Day, 2016). Literature regarding centrifugal compressors surge and stall performance is limited, therefore there is need for more research.

1.4 OBJECTIVES

The main objective was to develop and simulate performance of gas turbine compressors running on syngas derived from coal. This objective was achieved via the following specific objectives:

- To design a gas turbine compressor for compressing coal syngas using ANSYS.
- To determine the performance of the compressor based on variations of flow conditions, and test the influence of rotational speed on compressor instabilities using syngas.
- To compare the flow behaviour of syngas with air and identify onset of instabilities within the compressor.

1.5 JUSTIFICATION

Coal has been used to provide energy for heating and cooking. The traditional mechanism to convert coal to electricity has brought negative impacts on the envi-

ronment and humankind. Coal is converted to syngas and used in the production of methanol(Xu, 2017). This conversion of coal to syngas reduces the emission of GHG, and reduces diseases like lung cancer and heart problems that are brought about by pollution. The syngas produced can be compressed and fed into a gas turbine for power generation. Therefore, as the need for clean and renewable energy increases, coal gasification in power generation is a step towards sustainable power generation as renewable sources of energy are developed.

This research contributes important information for the power generation sector to utilize as it diversifies energy sources such as Ministry of Energy. Manufacturing, one pillar of the big 4 agenda set by the government of Kenya 2017, relies heavily on reliable energy generation and utilization.

There is need to provide more information on the behaviour of syngas in gas turbine compressors and compare its behaviour with that of air. Air is used as a baseline since extensive research has been done on it. The findings will contribute to increase in utilization of syngas in power generation systems.

1.6 OUTLINE OF THESIS

This thesis has 5 chapters. The current chapter is an introduction to the existing problem and what has been done to mitigate these problems. Literature review is chapter 2 and in it, existing theories on centrifugal compressors, and syngas utilization have been expounded. Chapter 3 is experimental design and methodology where the centrifugal compressor is designed and the flow parameters are simulated. Results and discussion are discussed in chapter 4. Chapter 5 presents conclusions and recommendations.

CHAPTER TWO

LITERATURE REVIEW

2.1 INTRODUCTION

Gas turbine engines can be used for power generation. Even though most gas turbine engines combust kerosene as fuel, syngas can be used as a substitute. Coal has been used as a source of energy, for cooking, and heating, for several decades. Traditional use of coal has led to pollution and as a result, global warming. One of the clean ways for using coal is through gasification. Gasification is a process that converts low quality fuels to valuable ones. Research on performance of centrifugal compressors using syngas is limited. This chapter reviews research that has been conducted on the use of syngas in centrifugal compressors. This has been done to determine the challenges associated with flow instabilities in centrifugal compressors using syngas as a working fluid.

2.2 GAS TURBINE CONCEPT

A simple gas turbine comprises of a compressor, combustor, and a turbine. The compressor increases the pressure of the operating fluid. The fluid then moves to the combustor where it is ignited, and then to the turbine where it is expanded and its energy is used to turn the turbine. In power generation, the turbine-compressor shaft is coupled to a generator to produce electricity(Spittle, 2003). Gas turbines can operate with either axial compressors or centrifugal compressors. Figure 2.1 shows a simple gas turbine concept.

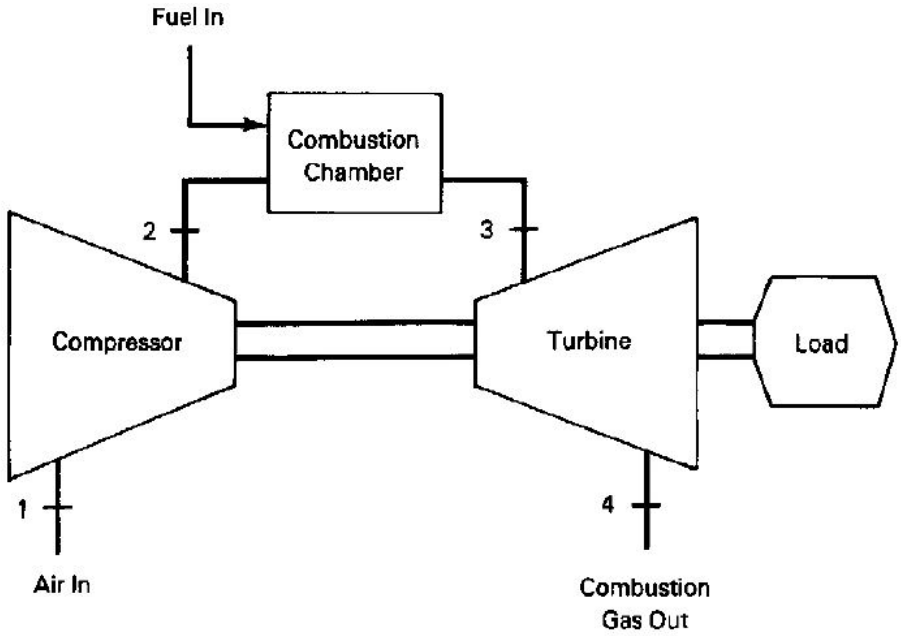

Figure 2.1: Schematic Diagram of an Open Gas Turbine

2.2.1 Centrifugal Compressors

Centrifugal compressors comprise of impeller, hub, shroud, diffuser, and inlet guide vanes as shown in Figure 2.2. The impellers are shrouded, unshrouded, forward swept, or backward swept.

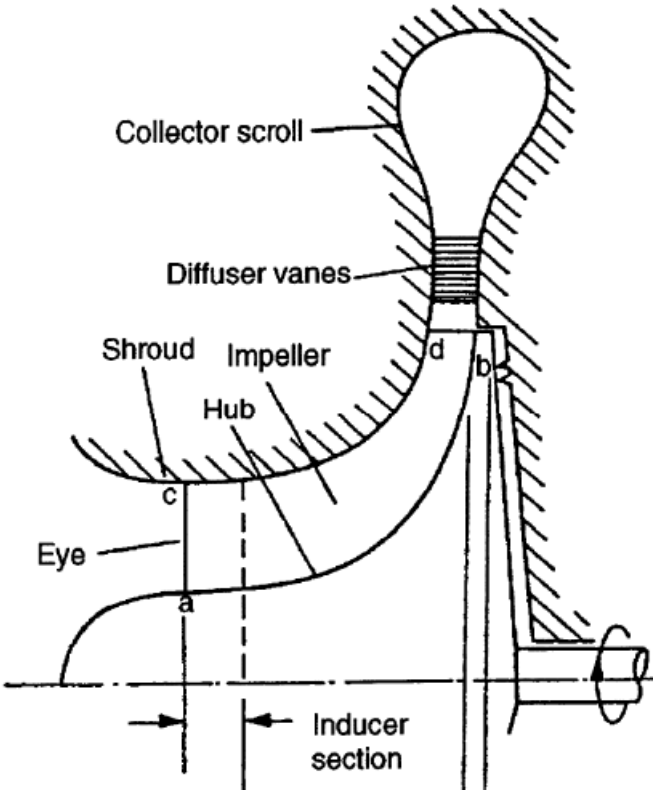

Figure 2.2: Centrifugal Compressor Parts (Zemp, 2006/2007)

Figure 2.3 shows example of blade sweeping. Blade sweep is the angle at which the trailing edge of an impleller blade is inclined at. If the sweep is 90^0, the blade is radial, if it is less than 90^0, it is backward swept and if it is greater than 90^0, it is forward swept.

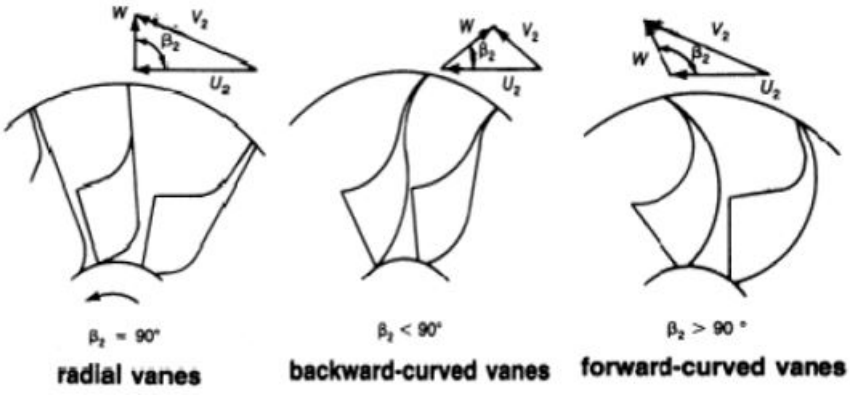

Figure 2.3: Centrifugal Compressor Impeller (Nagpurwala, n.d.)

The operating range and performance parameters governing the compressor characteristics, i.e. pressure ratio, mass-flow rate, and efficiency are commonly described in a compressor specific operation map. The obtainable boost pressure is given as ratio of the total pressure $p_{0,2}$ at the compressor outlet to the total pressure $p_{0,1}$ at the compressor inlet and illustrated as function of mass flow rate $\dot{m}$ and rotational speed n as shown in Figure 2.4.

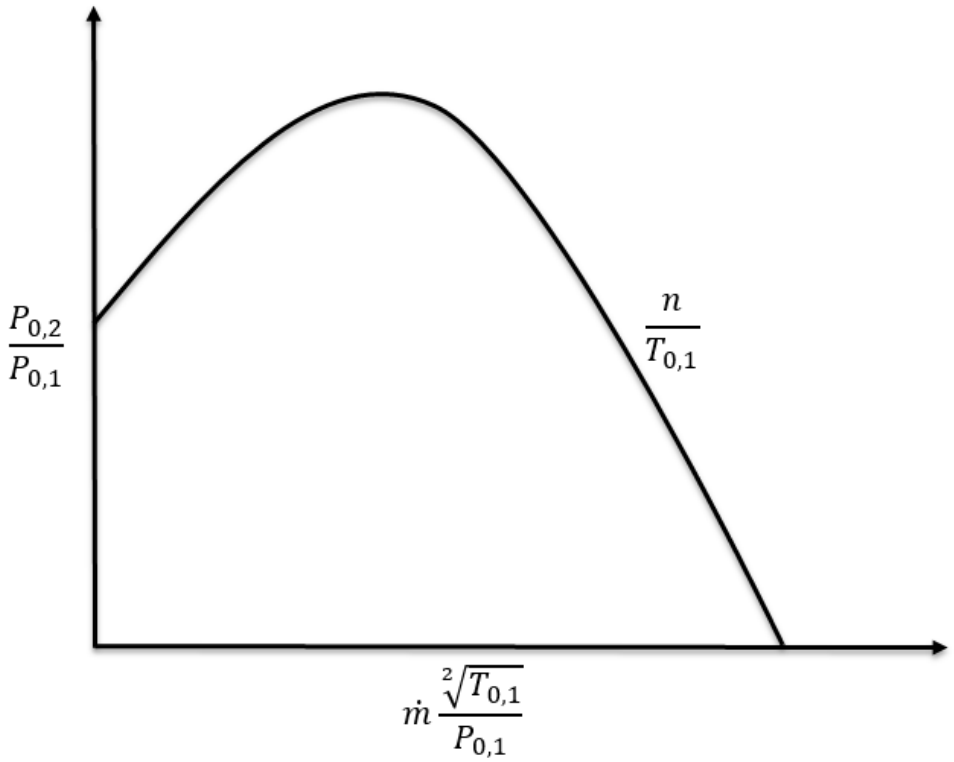

Figure 2.4: Compressor Map (Zemp, 2006/2007)

Centrifugal compressors can attain higher pressure ratios at one stage than axial compressors, and can be used where high speeds are required(Peirs, 2004; Banpurkar, 2015). Flow inside centrifugal compressors shows complex three-dimensional features due to compact structure, radial blade profiles, and strong adverse pressure gradients, especially for high pressure-ratio compressors(Xinqian, 2015).

2.3 FLOW INSTABILITIES IN CENTRIFUGAL COMPRESSORS

Surge and choke are flow instabilities encountered in centrifugal compressors. Surge is an unstable condition which causes flow reversal and pressure fluctuations(Boyce, n.d.). Surge can also be defined as a flow instability affecting the entire compressor, which can cause large vibratory stresses in the blades and lead to breakdown of its operation. Surge is a phenomenon of air stalling with partial flow reversal in the compressor(Semlitsch, 2016). Kurz et al.(Kurz, 2011) defined choke as a blockage experienced in the blade flow passages that occur during high flowrates. Surge and stall negatively affect the efficiency of the compressor.

The effects of surge include exponential temperature increase, process instability, potential machine trip, process shutdown and machine damage. Surging causes machine degradation which leads to reduced compressor life and lower efficiency. Surge is the result of an excessive increase in the resistance of the system while the compressor is operating at a certain speed. It may occur in either at the impeller or at the impeller-diffuser interface.

Surge occurrence is affected by how complex the compression system is such as increase in impeller blades. Few surge cycles can be tolerated by centrifugal compressors as long as the impulse or energy of the reversed flow is small in relation to the mass of the compressor rotating assembly(Almasi, 2012). The intensity of a surge tends to increase with increased gas density.

Bernhard et al.(Semlitsch, 2016) analysed flow through a centrifugal compressor with a ported shroud and a vaneless diffuser. The mass flow rate was reduced gradually from a stable operation range to unstable operating range. Modal decomposition was used to characterise the flow leading to surge. The centrifugal compressor used had 10 main blades with no splitter blades and the blades were at a backsweep angle of 25^0. Large Eddy Simulation LES was used to analyse flow leading to surge. Surge started to occur at a mass flowrate of 0.105 kg/s. At this low mass flow rate,

velocity reduction near the diffuser walls was observed. Although the aim was to use a ported shroud to allow for back-flow in the compressor, the cavities of the shroud disturbed the flow at the compressor inlet and a non-uniform flow field developed towards the blades.

Munzer et al.(Shehadeh, 2017) designed a centrifugal compressor as part of a microturbine which would operate at 60,000 RPM and generate 60 kW. This was done using non-linear optimization code. With this code, it was possible to determine principle geometric parameters of the impeller and the number of impeller blades in the compressor. Vaneless diffuser and the volute were designed by applying conservation equations and assuming an isentropic flow. Munzer et al. (Shehadeh, 2017) did not simulate or test the performance of this compressor therefore the instabilities occurring in the system were not determined.

Zheng et al.(Xinqian, 2015) investigated the flow instabilities in a centrifugal compressor with a vaneless diffuser. High-response pressure probes were used to capture the change in conditions within the compressor at high speeds. At speeds of less than 70% of the maximum speed and at low mass flowrates, stall was induced at the impeller inlet. When the flowrate was further reduced , the stall became surge and this surge extended to the diffuser. It was also observed that at 70% of the maximum speed, mild surge emerged. Zheng et al. concluded that at different operating conditions, different surge patterns occur. The medium used was air. This study propose use of syngas as an alternative to air, on evaluation of discussed surge.

Kurz et al.(Kurz, 2011) simulated flow in a multistage centrifugal compressor. The aim was to investigate the compressor's operation during choke and resultant axial thrust loading. The compressor had 19 main blades. Authors found that vaneless diffuser has no effect when a compressor is operating in choke. From their analysis, as inlet flow coefficient increased, the thrust bearing temperature also increased. The finally concluded that operating a centrifugal compressor in choke was not a problem if the balance piston provides adequate thrust and if the impeller blade was

strong enough to withstand the alternating stresses.

Nabil et al.(Mostafa, 2006) reviewed prediction of surge and rotating stall in a compressor. The models reviewed were linear lumped parameters,non-linear lumped parameters, and distributed parameters "blade-to-blade solutions". The non-linear lumped parameters and distributed parameters were able to predict surge and rotating stall in a one-stage centrifugal compressor. The recommendation was to develop complex non-linear lumped parameters and distributed parameters for analysing multi-stage compressors with increased simulation accuracy.

Figure 2.5 shows how surge is brought about in a compressor at different time intervals. At the first interval, the flow is stable. As the intervals progress, the stable conditions reduces and surge occurs. At the last time-step, some blade passages are blocked like blade 2 and 5 and 18 (region indicated by blue). This blockage indicates surge (Trbinjac, 2015).

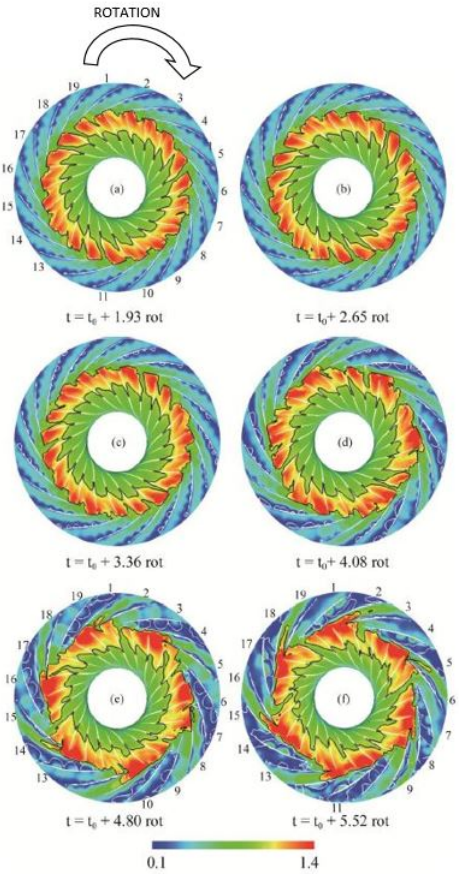

Figure 2.5: Surge Inception in a Centrifugal Compressor (Trbinjac, 2015)

Surge can be minimized and avoided by use of anti-surge systems. These can either be valves that drain off some of the fluid or programmable units that operate independently(Almasi, 2012). When the compressor is operated at high flow rates, chocking occurs. Surge originates in the diffuser and is caused by surface friction that brings about restriction of flow. Surge also occurs when the compressor operates at low flow rates. Surging causes mechanical vibration which has a potential to cause compressor failure.

Stall is closely related to surge and it affects the impeller. It occurs when the radial velocity of the gas entering the diffuser or efficiency of the diffuser are too low therefore the flow collapses as it passes through the diffuser. Stall is more prevalent on low flow impellers and is likely to occur on high pressure low flow applications. It

tends to onset as the flow approaches surge. There are three types of stall: rotating stall, blade-impeller stall, and stall flutter. Stall flutter results from blade-impeller excitation. It occurs when the flow around a blade-impeller is stalled, causing an excitation and it is the main reason for inducer vane failures in centrifugal compressors as shown in Figure 2.6. Rotating stall is the most common stall found in compressors(Almasi, 2012).

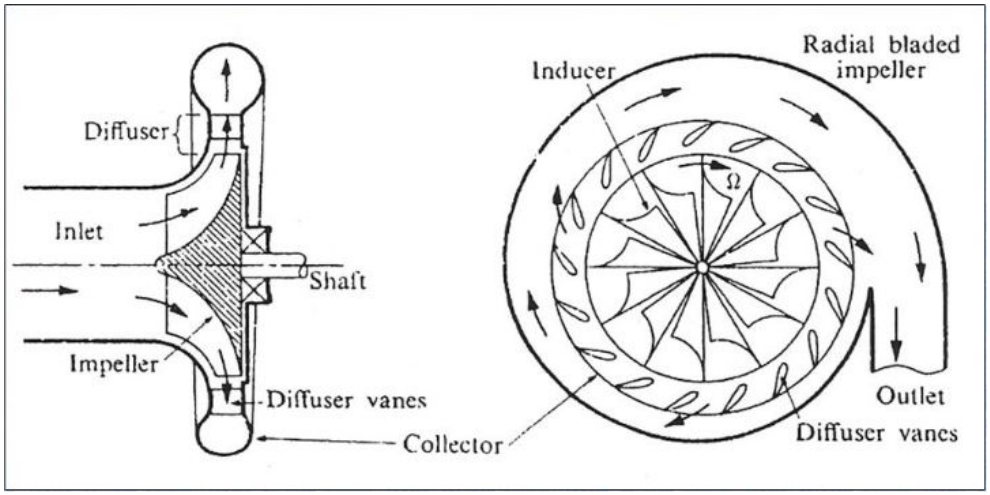

Figure 2.6: Inducer Vane (Ali, 2016)

2.4 GEOMETRIC CONFIGURATION OF CENTRIFUGAL COMPRESSORS

Some of the key features influencing performance of compressors are impeller profile and the their tip clearance. Their role and how flow conditions influence their performance is presented in the following subsections.

2.4.1 Impeller Profile

In compressors, the most crucial element is the impeller. This is because the impeller transfers kinetic energy to the working fluid(Banpurkar, 2015). Blades should

be designed in a way that minimises flow losses.Variables in the impellers that influence efficiency, operating range and blade stress in the compressor are: impeller tip diameter, back-sweep angle, tip/exit) depth, inducer inlet angle and rotor eye, blade leading edge shape, curvature of blade shape and, tip clearance.
The tip diameter is fixed to obtain required pressure ratio. The larger the tip diameter, the higher the efficiency. The tip depth influence on compressor performance has not been researched extensively(Benini, 2003). Blade sweep reduces base load at leading edge but increases it at trailing edge. Blade lead increases the pressure on the pressure surface. Forward swept blades have a better performance and increase compressor efficiency by almost 1% while backward swept blades increase the efficiency by 0.5%. Forward swept blades reduce the interaction between the shockwave and the casing wall boundary layer while the backward swept blades reduce chocking flow rate. Therefore both sweep and lean should be present in a blade design since they improve chocking flow rate and efficiency in various operating ranges of a compressor(Neshat, 2015).

Neshat et al.(Neshat, 2015) investigated the effects of blade sweep and lean on the performance of compressor. They did this using numerical solutions and found that an impeller blade with back sweep is less affected by lean angle, has reduced stall margin, and chocking flow rate reduced by 1.5%. For a blade with forward sweep, the stall margin increases and chocking flow rate increases by 0.18%. They concluded that forward swept blades influence upstream flow while backward swept blades affect the rotor stages downstream. He did not establish the angle of the backward swept blade that would generate optimal flow.

2.4.2 Tip Clearance

Tip clearance does have a significant influence on the efficiency of uncovered impellers. Tip clearance is the distance between impeller blade and compressor casing.

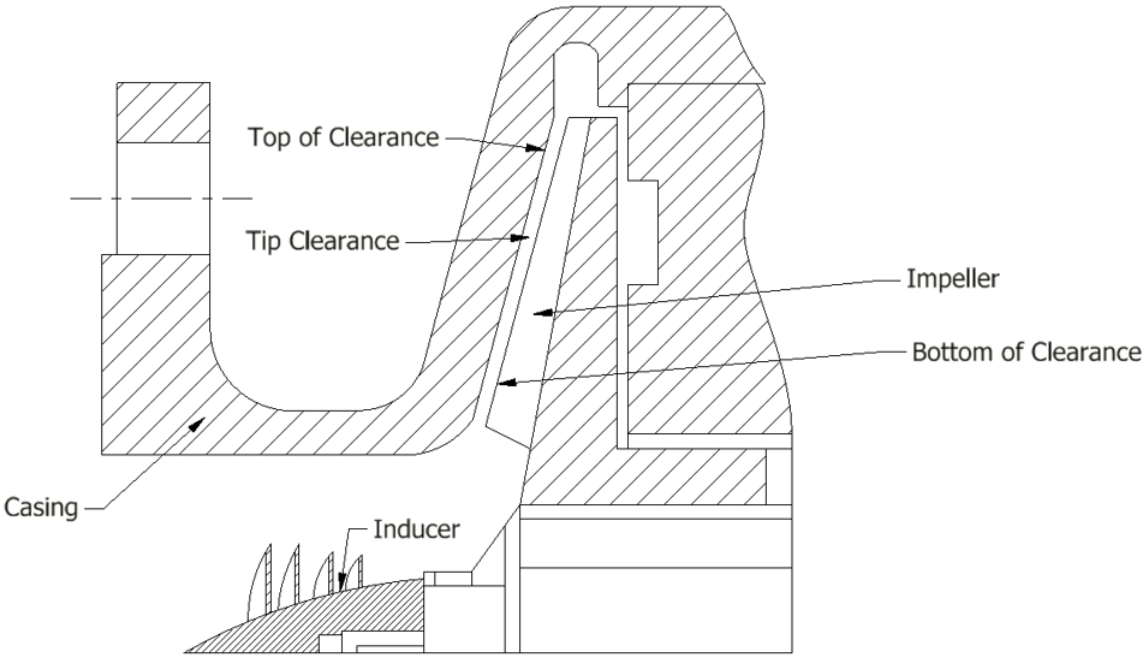

Figure 2.7: Tip Clearance (Jia, 2014)

Syed et al.(Noman, 2006) investigated the effect of impeller blade tip clearance using detailed numerical simulations. He connected an impeller and diffuser to a rotor stator boundary using frozen rotor approach and overall performance from clearance tips of 1mm to no gap. In his findings, maximum impeller efficiency was at 0.1-0.2mm tip clearance. They did not determine whether the tip clearance is effective in forward swept or backward swept impellers.

Matthias et al.(Schleer1, 2008) sought to increase the knowledge on tip clearance and how it affects stability in the compressor. Their aim was to investigate large tip clearance and its effect on the onset of stability in a centrifugal compressor. The findings were that pressure builds up at the radial part of the compressor due to centrifugal forces. Also, reduced tip clearance ratio improved impeller performance.

Tip clearance effect on the pressure ratio in the centrifugal compressor was not proven.

2.5 WORKING FLUIDS IN GAS TURBINE SYSTEMS

Syngas is obtained from gasification of plant biomass or waste products. It is composed of gas elements such as H_2, CO, and CH_4 and inert diluents such as N_2 and CO_2. These diluents influence the ignition of syngas by reducing the temperature of the air/fuel mixture heading to the spark and hence reducing the initial flame kernel.

Gasification is a process that converts low quality fuels to valuable ones. The process can be applied to biomass as well as coal. In biomass gasification, tar is obtained during pyrolysis thus has to be converted to lighter gases like CH_4, CO and water(Filippisa, 2015). Filippis et al.(Filippisa, 2015) used olive husks in an industrial scale plant. The syngas produced was fed to an internal combustion engine. Their aim was to remove tar produced during gasification using a second reactor. They was able to remove more than 50% of the tar produced. With the removal of tar, they proved that it is possible to remove impurities earlier on in the gasification process in order to reduce the energy needed for purification. The syngas produced was fed to an internal combustion engine which generated 60kWe and an efficiency of 25% was achieved.

Gas generated by gasification of coal comprises of H_2 and CO and small amounts of CH_4 and higher order carbons. Impurities such as sulphur, alkali species, and small particulate matter are also present but can be eliminated by employing a cleaning process of the syngas(Gibbons, 2007).

Suhui et al.(Li, 2014) investigated the behaviour of syngas in spark ignition using gas turbine start up conditions, and the effects of the syngas fuel composition and air

flow on ignition performance. They discovered that syngas has better ignition performance as compared to natural gas though one of the hinderance of using syngas in gas turbine is its change in composition and heating value. They also found out that air flow affects heat transfer from spark to the surrounding reactants and to the incoming air-fuel-mixture. Therefore, high air flow velocity impinges on ignition(Li, 2014). In this research, they did not use a mixture of natural gas and syngas but rather syngas alone hence proving that syngas can be used in gas turbine engines. Syngas has to have high H_2 content for it to ignite well.

Flashback of premixed H_2/air swirling flames is another problem experienced when using syngas in gas turbine systems. This is because of the high H_2 content in syngas (Li, 2014). Diffusion flame approach can be used to eliminate flashback in the gas turbine. There exist syngas fired turbines using diffusion flame designs operating with diluent addition. This is because diluent allows control of the primary zone temperature.

Another factor to be considered while using syngas in gas turbine systems is the emission during combustion. In their paper, Kent et al.(Casleto, 2008) discusses the need to remove fuel contaminants in syngas such as sulphur, hydrogen, ash, and heavy metals. They stated that gas turbine systems running on syngas can achieve an efficiency of 40% and NO_x emission of 15 ppm at 15% O_2. In their paper, they discussed that crude syngas temperature should first be lowered using heat exchangers, then it should be passed through a gas scrubber to remove slag, sulphur, and ammonia. The NO_x emission would be removed in the exhaust of the gas turbine system rather than dealing with it in the combustor. For future syngas combustion he gave examples of oxy-fuel, chemical looping, fuel cells, and hybrids that would be used(Casleto, 2008).

According to Wang et al. (Wang, 2012), syngas has lower calorific value than natural gas therefore the mass flowrate of the syngas has to be more in the turbine therefore increasing the discharge pressure of the compressor.

For this research, gas elements of syngas were used for simulation. These values were used as a representation of coal available world wide including from Mui basin.

2.6 GAPS IDENTIFIED IN LITERATURE

There exist literature on how surge, stall, and choke affect the compressor performance. Several gaps have been identified in the literature and these will be key areas that will be focused on during the study of centrifugal compressors. Some of these gaps are:

1. Surge, choke and stall affect flow of diffusers and there is need to reduce their impact on performance of diffusers.

2. It is essential to study the onset of surge in a backward swept impeller, and how the angle of sweep reduces or increases surge occurrence.

3. How the configuration of diffusers affect the stability. It is therefore necessary to study the use of vaned and vaneless diffusers in a bid to minimize instability, their effects in the centrifugal compressor to determine which diffuser is suitable for which sweep.

4. The condition of syngas is important in performance of gas turbines. It is essential that effect of purification and blending with natural gas be studied further.

CHAPTER THREE

METHODOLOGY

3.1 INTRODUCTION

The aim of this research was to come up with a centrifugal compressor as part of a gas turbine plant for electricity generation. Centrifugal compressor was chosen because it can attain higher pressure ratios at one stage than an axial compressor, and it can be used where high speeds are required(Peirs, 2004; Banpurkar, 2015). The fluid used in the gas turbine was syngas. The centrifugal compressor was designed using ANSYS workbench student version. The geometrical specifications were input into Vista CCD (Centrifugal Compressor Design) which generated the centrifugal compressor. This information was transferred to Blade Gen, then to mesh and simulation was done using Ansys CFX, where input parameters were set and the conditions modelled. The design details and how simulation was done are presented in this chapter.

3.2 COMPRESSOR IMPELLER DESIGN

ANSYS (Analysis of System) is a simulation tool that contains various systems which include fluid flow systems, static structural systems, and rigid dynamic systems to name a few. These components have been written using FORTRAN, C and C++.

A centrifugal compressor comprises of inlet, outlet, impeller blades and diffuser. In this study, focus was on the impeller since it imparts the fluid with momentum and instabilities like surge and stall also occur at the impeller. The centrifugal compressor was modelled using Vista CCD (Centrifugal Compressor Design) which is an

inbuilt component system in ANSYS.

3.2.1 Geometric Modelling

The computational space was modeled as a vaneless diffuser consisting of an unshrouded impeller having 15 impeller blades. This was based on the criteria from previous studies showing an increase in efficiency for blade number between 12 and 15 and the optimum blade number was 15(Rodgers, 2000; Srinivas, 2014).

Further the selection of an unshrouded impeller was based on the criteria that unshrouded impellers have higher tip speeds which result in an increase of volume flow and head(Ludtke, 2004). Micro-gas turbines have the advantages of being light weight, having greater efficiency, low capital cost, and a small number of moving parts.

The geometrical specifications for the centrifugal compressor are given in Table 3.1 below:

Table 3.1: Compressor Values Input in Vista CCD

Geometry	**Values**
Diffuser Type	Vaneless
Impeller type	Unshrouded
Hub diameter	30 mm
No. of main blades	15
Backsweep angle	45^0

Table 3.2 shows the generated values for the centrifugal compressor exit.

Table 3.2: BladeGen Generated Compressor Values

Geometry	**Values**
Impeller exit tip diameter	113.23mm
Impeller exit tip chord	6.4378mm
Blade tip speed	533.57 m/s
Blade tip Mach number	1.568
Shroud diameter	73.005 mm

Figure 3.1 shows the geometry of the impeller blade with a surface area of $1,959.4mm^2$ and a volume of $985.35mm^3$.

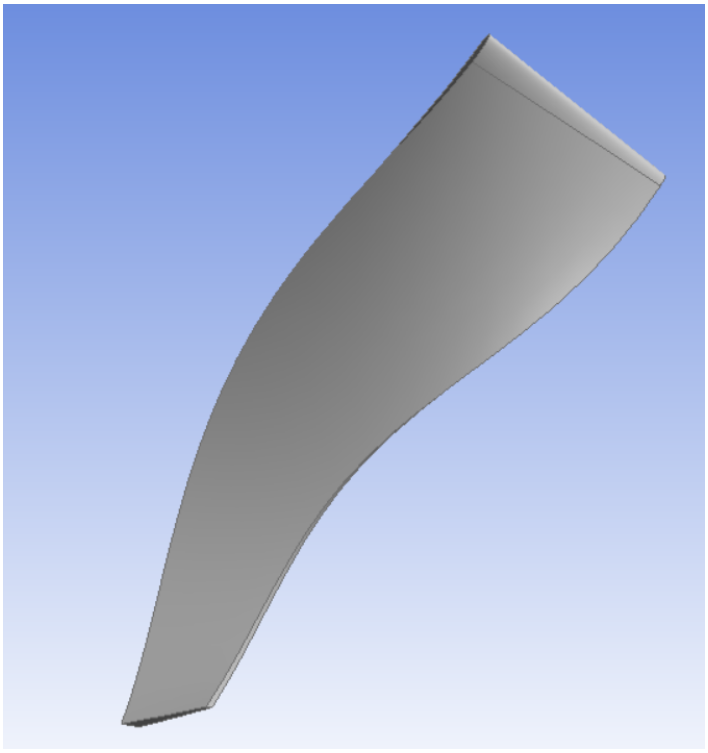

Figure 3.1: Geometry of Compressor Impeller Blade

3.2.2 Impeller Blade Generation

Compressor data was transferred from Vista CCD to BladeGen. This is because data cannot be transferred directly from Vista CCD to mesh in Ansys. Initial blade set-up was defined and this included the number of blades. Figure 3.2 shows the meridional view of the centrifugal compressor. The blade shape was defined by the number of layers and in this case, there were 4 layers. This number was generated automatically in BladeGen.

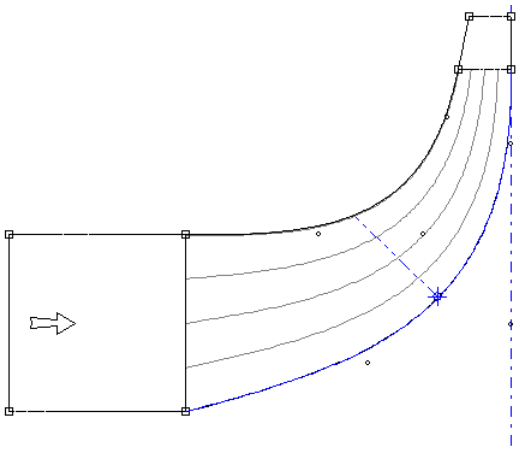

Figure 3.2: Meridional View of the Centrifugal Compressor

Figure 3.3 shows the auxiliary view of the centrifugal compressor.

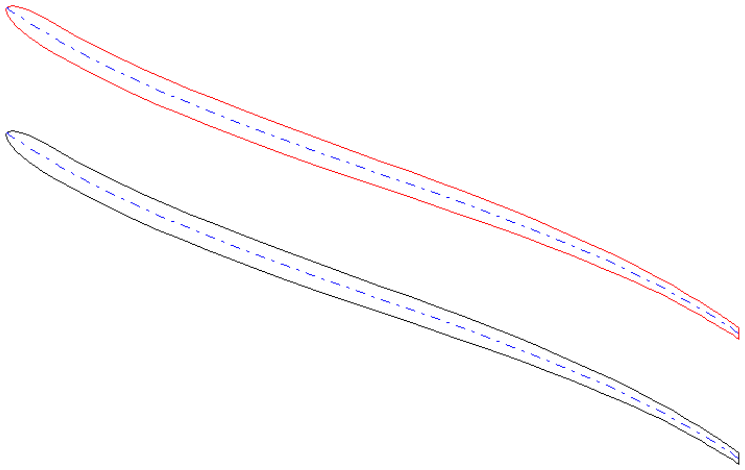

Figure 3.3: Auxiliary View of the Centrifugal Compressor

With the data from Vista CCD, the blade and layer parameters were generated automatically in BladeGen.

Figure 3.4 shows the complete compressor, the impeller blades, disc casing, and outlet. The complete compressor was used in the simulation. Setting selected for the compressor was steady state.

Table 3.3: Blade Values

Type	Values
Airfoil area	$128.645mm^2$
3D meanline length	70.7753mm
Camber length	70.7763 mm
Meridional length	64.1001
Stager angle	24.7^0
Solidity	2.97445
Pitch cord ratio	0.336197

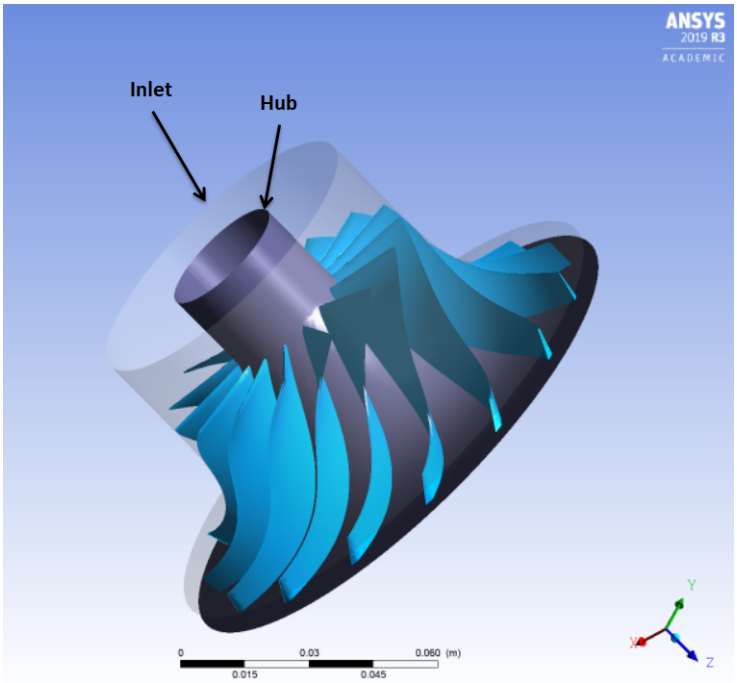

Figure 3.4: Compressor Design

3.3 MESH GENERATION

Upon identification of a computation domain, it was necessary to discretize the domain. This entailed discretization of domain into small control volume domains known as mesh cells. For the regions having severe flow gradients, it was essential to refine the mesh to capture boundary layer near wall region.

Figure 3.5 shows fluid flow channel before meshing while Figure 3.6 shows the meshed domain.

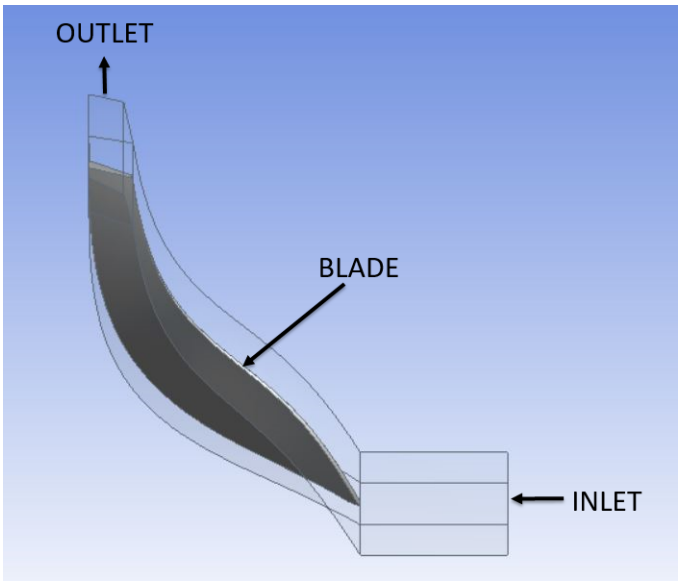

Figure 3.5: Fluid Flow Extracted from Figure 3.4

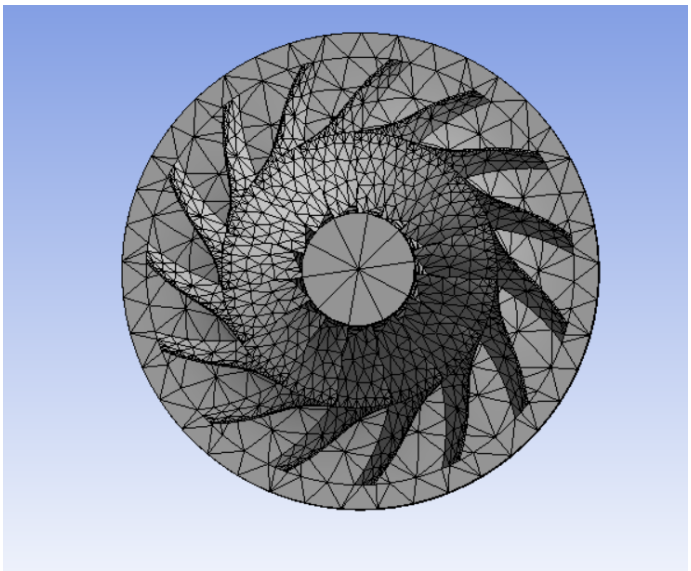

Figure 3.6: Meshed 3D Centrifugal Compressor

The type of mesh generated was tetrahedron which are unstructured grids preferred for a complex shape geometry and also enjoy a high level of flexibility control of grid parameters such as cell shape and size. Solution of discretized equations can be applied to arbitrarily shaped computational domains(Mavriplis, 1997; Kovalev, 2005). A 2^{nd} order element refinement was set under near the impeller wall.

Mesh size was varied by changing the output smoothing from low, medium and high

and refinement was increased from 1 to 3. Physical preference selected was CFD while solver preference selected was CFX.

Figure 3.7 shows tetrahedron mesh and the refinement near the blade while Figure 3.8 shows hex mesh and the blade refinement.

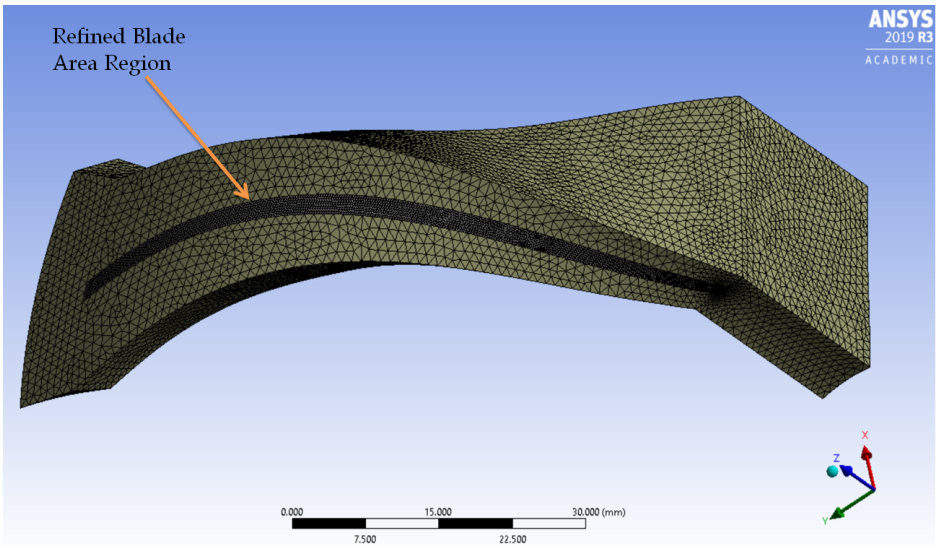

Figure 3.7: Refined Tetrahedron Mesh at the Blade Area

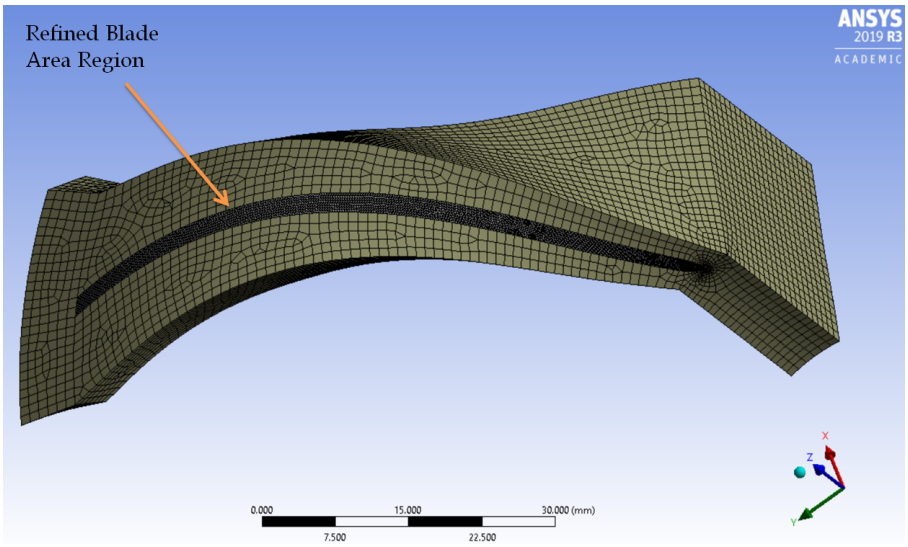

Figure 3.8: Refined Hex Mesh at the Blade Area

There exist several mesh elements available in mechanical mesh tool for 3D objects. Tetrahedrons and hex dominant meshing methods were investigated. Ta-

ble 3.4 shows that tetrahedron method with CFD as the analysis type, also known as physics preference in meshing, had more nodes and elements than any other category and this was the basis for selecting it.

Table 3.4: Grid Sensitivity Criteria

Method	Physics Preference	Nodes	Elements
Tetrahedon	CFD	931077	647584
Hex dominant	CFD	605811	300732

3.4 GOVERNING EQUATIONS

Flow conservation equations were solved to simulate the behavior of the fluid across the compressor. These flow equations included mass, momentum, species conservation and energy equations. These equations were expressed on a cartesian coordinate system(Zikanov, 2010).

1. Mass conservation/ continuity equation.

$$\frac{\partial \rho}{\partial t} + \nabla.(\rho V) = 0 \tag{3.1}$$

   where ρ was the density expressed in kilogram per cubic metre (kg/m^3), t was time expressed in seconds(s), V was the velocity vector expressed in metres per second (m/s), and ∇ was divergence of the flowing fluid.

2. Momentum conservation equation.

$$\rho \frac{D}{Dt}(V) = \rho[\frac{\partial}{\partial t}(V) + (V \cdot \nabla)V] \tag{3.2}$$

   where ρ was density, V was the velocity expressed in metres per second (m/s), and μ was the viscosity coefficient.

In the x-direction:

$$\rho\frac{Du}{Dt} = \rho f_x - \frac{\partial p}{\partial x} + \frac{\partial}{\partial x}\left[\mu\left(-\frac{2}{3}\nabla.V + 2\frac{\partial u}{\partial x}\right)\right] + \frac{\partial}{\partial y}\left[\mu\left(\frac{\partial v}{\partial x} + \frac{\partial u}{\partial y}\right)\right] + \frac{\partial}{\partial z}\left[\mu\left(\frac{\partial w}{\partial x} + \frac{\partial u}{\partial z}\right)\right] \tag{3.3}$$

In the y-direction:

$$\rho\frac{Dv}{Dt} = \rho f_y - \frac{\partial p}{\partial y} + \frac{\partial}{\partial y}\left[\mu\left(-\frac{2}{3}\nabla.V + 2\frac{\partial v}{\partial y}\right)\right] + \frac{\partial}{\partial x}\left[\mu\left(\frac{\partial v}{\partial x} + \frac{\partial u}{\partial y}\right)\right] + \frac{\partial}{\partial z}\left[\mu\left(\frac{\partial w}{\partial y} + \frac{\partial v}{\partial z}\right)\right] \tag{3.4}$$

In the z-direction:

$$\rho\frac{Dw}{Dt} = \rho f_z - \frac{\partial p}{\partial z} + \frac{\partial}{\partial z}\left[\mu\left(-\frac{2}{3}\nabla.V + 2\frac{\partial w}{\partial z}\right)\right] + \frac{\partial}{\partial x}\left[\mu\left(\frac{\partial w}{\partial x} + \frac{\partial u}{\partial z}\right)\right] + \frac{\partial}{\partial y}\left[\mu\left(\frac{\partial w}{\partial y} + \frac{\partial v}{\partial z}\right)\right] \tag{3.5}$$

where ∇ was divergence, V was the velocity expressed in metres per second (m/s), f was net force (N) per unit mass (kg), and μ was the viscosity coefficient.

3. Energy Conservation Equation.

$$\rho C\left(\frac{\partial T}{\partial t} + V.\nabla T\right) = \kappa\nabla^2 T \tag{3.6}$$

where ρ was density expressed as kilogram per cubic metre (kg/m^3), C was the specific heat expressed as Joule per kilogram Kelvin (J/kgK), T was the temperature field expressed in Kelvin (K) while κ was conduction coefficient constant. Energy conservation equation was necessary because of the heat generated during compression.

4. Equation of State(Zikanov, 2010)

$$\frac{p}{\rho} = RT \tag{3.7}$$

where p was pressure expressed in Pascal (Pa), ρ was the density expressed in kilogram per cubic metre (kg/m^3), R was the ideal gas constant, and T was absolute temperature expressed in Kelvin (K).

The assumptions made were that the flow was 3-dimensional, viscosity and specific heat capacity were constant, all species followed the perfect gas laws and there was no radiation.

3.4.1 Reynold-Averaged Navier-Stokes Equation (RANS)

Reynolds time averaging was applied to the governing equations and resulted in the Reynolds-Averaged Navier-Stokes equation . The continuity equation remained the same but the momentum equation changed. RANS is the oldest method of turbulence modelling and some of its advantages are simplicity, low computational cost relative to Direct Numerical Simulations (DNS) and Large-Eddy Simulations (LES)(Zikanov, 2010). Some of the assumptions made were that the flow was incompressible, fluid flows were turbulent, and components of velocity and pressure were represented in their mean and fluctuating values. The momentum equations became (Zemp, 2006/2007):

$$\rho\frac{\partial u_i}{\partial t} + \rho\frac{\partial}{\partial x_j}(u_i u_j) = -\frac{\partial p}{\partial x_i} + \mu\nabla^2 u_i \tag{3.8}$$

where $u_i u_j$ are velocity time-averaged values.

Reynolds Averaged energy equation became(Zemp, 2006/2007):

$$\frac{\partial(\rho h_0)}{\partial t} + \nabla.\left(\rho\vec{U}h_0 + \rho\overline{u'h} - \lambda\nabla T\right) = \frac{\partial P}{\partial t} \tag{3.9}$$

where mean total enthalpy is

$$h_0 = h + \frac{1}{2}U^2 + k \tag{3.10}$$

U is the mean flow kinetic energy and k is turbulent kinetic energy given by:

$$k = \frac{1}{2}\overline{u'^2} \tag{3.11}$$

3.4.2 $k-\omega$ SST Turbulence Model

This model was selected due to its widespread application as it integrates features of both $k-\epsilon$ and $k-\omega$ model(Zikanov, 2010) while the analysis type selected was steady state. This resulted7 in more accurate predictions and less sensitivity to grid variations than $k-\epsilon$.

Modeled equation for turbulent kinetic energy k was:

$$\frac{\partial(\rho k)}{\partial t} + \frac{\partial(\rho u_j k)}{\partial x_j} = P - \beta\rho\omega k + \frac{\partial}{\partial x_j}\left[(\mu + \sigma_k\mu_t)\frac{\partial k}{\partial x_j}\right] \tag{3.12}$$

where ρ is density, P is pressure, ω is the turbulence frequency, k is the turbulent kinetic energy, and μ is the viscosity coefficient.

Modelled equation for specific dissipation rate was:

$$\frac{\partial\omega}{\partial t} + U_j\frac{\partial\omega}{\partial x_j} = \alpha S^2 - \beta\omega^2 + \frac{\partial}{\partial x_j}[(\nu + \sigma_\omega\nu_T)\frac{\partial\omega}{\partial x_j}] + 2(1-F_1)\sigma_{\omega^2}\frac{1}{\omega}\frac{\partial\kappa}{\partial x_i}\frac{\partial\omega}{\partial x_i} \tag{3.13}$$

3.4.3 Centrifugal Compressor Efficiency Equation

The efficiency of a centrifugal compressor is calculated as follows:

$$\eta_{CC} = \frac{IdealWorkInput}{ActualWorkInput} = \frac{(\frac{P_{02}}{P_{01}})^{\frac{\gamma-1}{\gamma}} - 1}{\frac{T_{02}}{T_{01}} - 1} \tag{3.14}$$

where

P_{02} is pressure at the outlet,

P_{01} is pressure at the inlet,

T_{02} is temperature at the outlet, and

T_{01} is temperature at the inlet.

3.4.4 Flow near Wall

The wall distance is used in several functions that control the transition between near- wall and free- stream models. Viscosity affected sublayer region is bridged by employing empirical formulas to provide near-wall boundary conditions for the mean flow and turbulence transport equations. These formulas connect the wall conditions to the dependent variables at the near- wall mesh node (Armin et al. 2006(Zemp, 2006/2007)). The logarithmic relation for the near wall velocity was obtained from:

$$u^+ = \frac{U_t}{u_\tau} = \frac{1}{k} ln(y^+) + C \tag{3.15}$$

where

$$y^+ = \frac{\rho \Delta y u_\tau}{\mu} \tag{3.16}$$

and

$$\mu_\tau = (\frac{\tau_\omega}{\rho})^{\frac{1}{2}} \tag{3.17}$$

u^+ is the near wall velocity, u_τ is the friction velocity, U_t is the known velocity tangent to the wall at a distance Δy from the wall, y^+ is the dimensionless distance from the wall, τ_ω is the shear wall stress, k is the von Karman constant and C is a log-layer constant depending on wall roughness (Armin et al. 2006(Zemp, 2006/2007)).

3.5 BOUNDARY CONDITIONS

Shown in Figure 3.9 is the fluid flow zone with one blade.

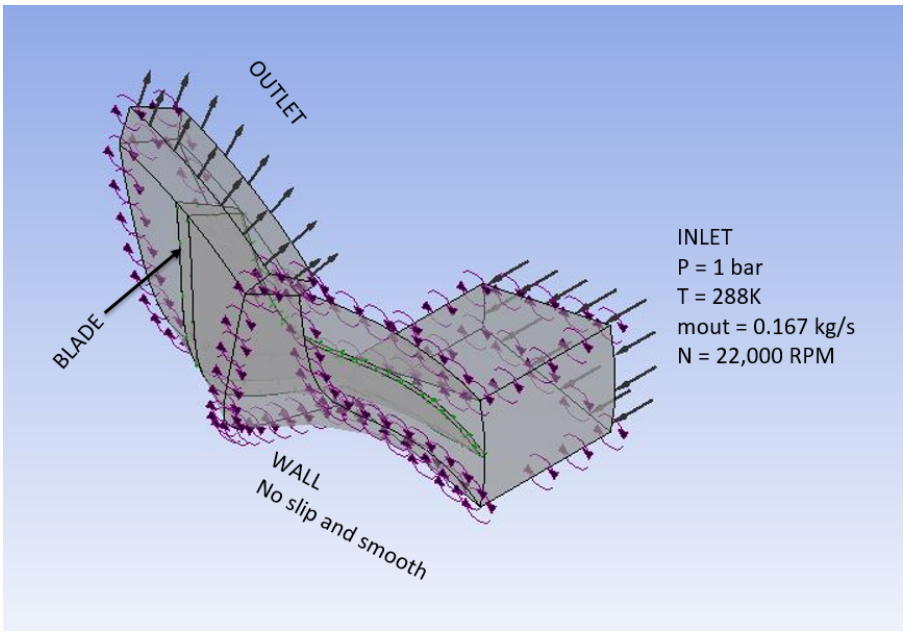

Figure 3.9: Boundary and Boundary Conditions

Table 3.5 shows the inlet parameters: Reference pressure helps to fix the pressure in the computational domain to a known value. The initial fluid used was air at a temperature of 288K. This was done to obtain a baseline for analysis and comparison with syngas. The centrifugal compressor was rotated at a speed of 22,000RPM.

Table 3.5: Inlet Parameters

Parameter	Values
Reference Pressure	10 bar
Total Pressure	1 bar
Total Temperature	288 K
Mass flowrate	0.167 kg/s
Rotational Speed	22,000 rpm

This value was obtained from previous studies which aimed to numerically investigate flow through compressor blades(Srinivas, 2014).

Rotational speed was selected as the independent parameter. It was reduced in steps 1,000RPM of upto 5,000 RPM. This is because there were no significant changes in decrements of less that 1,000RPM. As for mass flowrate, an initial mass flowrate of 0.167kg/s. This was done in order to compare the pressure contours obtained from simulation with those obtained from literature. Pressure contours were selected since they clearly indicate the pressure variations in the centrifugal compressor using different colors. Table 3.6 shows the syngas composition that was used in the

Table 3.6: Syngas Parameters

Gas	Material Group	Mass Fraction	Temperature
CO	Ideal Gas	0.2	288 K
H_2	Ideal Gas	0.8	288 K

compressor. The syngas was modelled as a gas comprising of two elements, CO and H_2. This was taken as a representation of syngas obtained from gasification of coal. Coal from Mui Basin could not be obtained therefore the syngas composition was obtained from literature.

CHAPTER FOUR

RESULTS AND DISCUSSION

4.1 OVERVIEW

This chapter presents findings from the simulation of compression of syngas flowing through a gas turbine compressor in order to analyze the behaviour and track any resulting instabilities if any. The performance of the compressor has been presented based on the structure of the flow field under the influence of independent variables such as syngas mass flow rate, inlet pressures and rotational speed of the compressor. Therefore this chapter contains the results and discussion of validation of the simulation; influence of inlet pressure, velocity and mach number on the performance of the compressor.

4.2 MESH SENSITIVITY ANALYSIS

Figure 4.1 shows the grid convergence study that was carried out to ensure that the grid was independent and discretization errors low. Low, medium and high grids were simulated and the efficiency plotted. Efficiency increased with increase in number of elements until 358679 element where it became constant. This showed that a solution independent of the mesh resolution had been reached and continual increase in elements did not have much effect on the efficiency. Therefore, high grids of 367878 were selected and their efficiency was maximum. The mesh sensitivity was carried out to determine the accuracy of the numerical results and their behaviour with varying cell numbers.

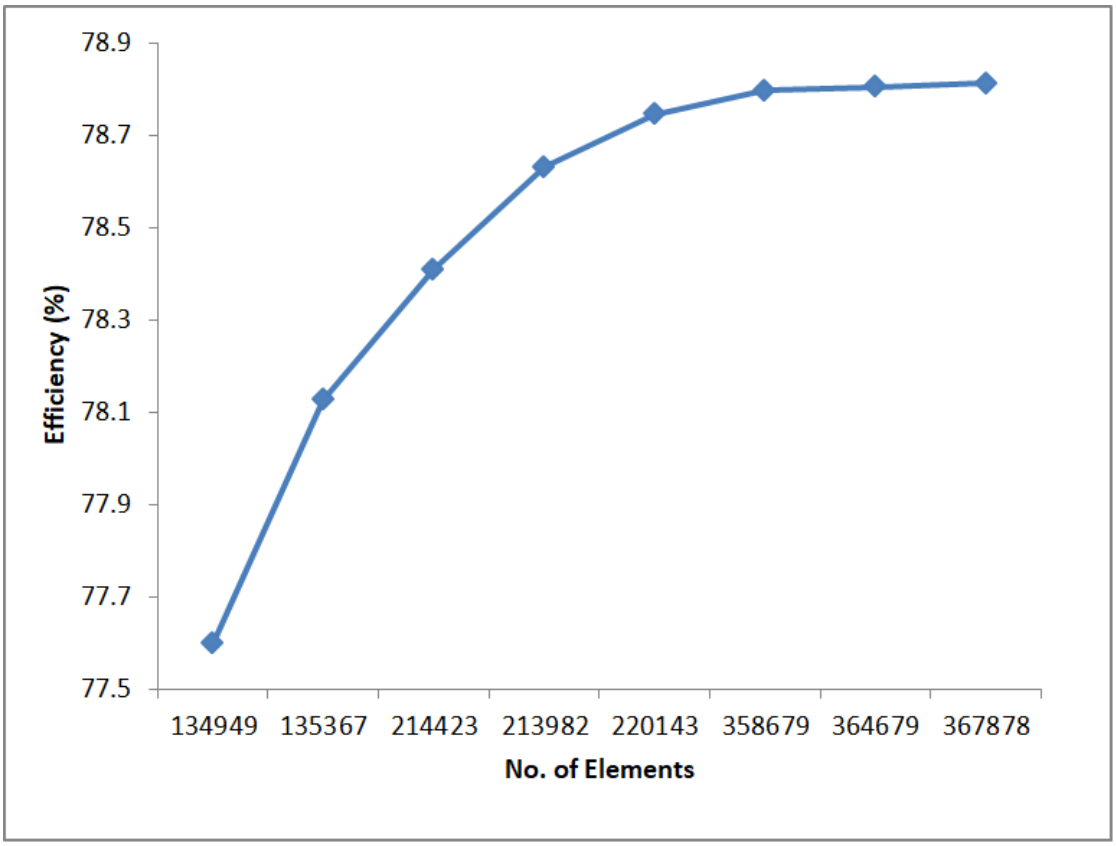

Figure 4.1: Mesh Independence Study to determine Accuracy of Numerical Results

Table 4.1 shows the variation in mesh size, the respective nodes and elements, and efficiency for each size.

Table 4.1: Mesh Size Variation

Grid	Nodes	Elements	Efficiency(%)
Low	257186	126587	77.67
Medium	280419	139205	78.4
High	752508	366258	78.75

4.3 COMPUTATIONAL CONVERGENCE

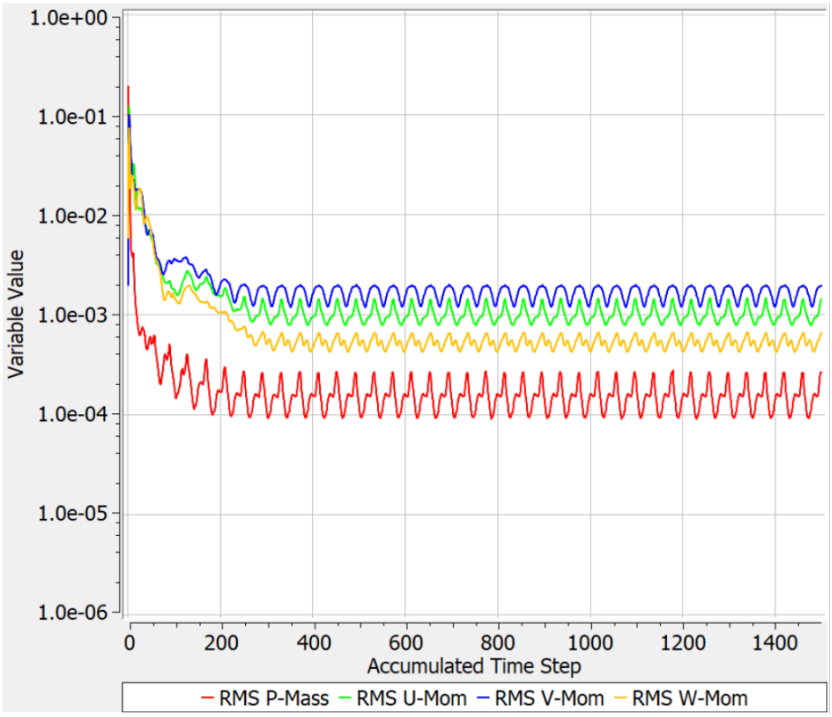

Figure 4.2: Convergence Trends for Mass and Momentum

Figure 4.2 shows grid convergence trends of air for mass and momentum. RMS P-Mass is the root mean square for mass, RMS U-Mom is the root mean square for momentum in X direction, RMS V-Mom is the root mean square for momentum in Y direction, and RMS W-Mom is the root mean square for momentum in Z direction. The convergence criterion associated with mass and momentum was achieved after 200 iterations. This showed that the solution of mass and momentum equations converged for a tolerance between $1.0e^{-}2.5$ and $1.0e^{-}4.5$. The convergence criteria for mass and momentum was approximated around $1.0e^{-}3.5$.

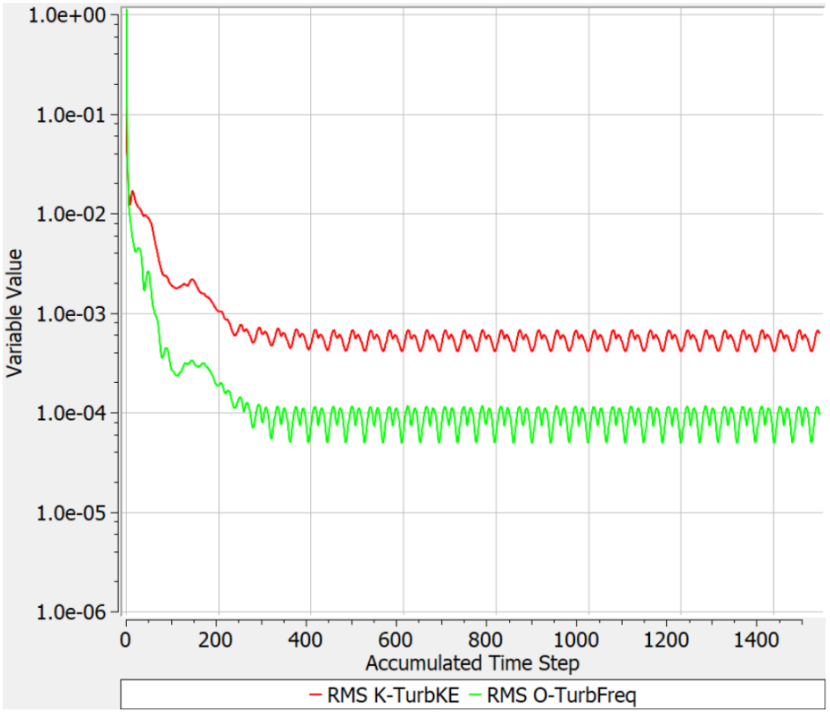

Figure 4.3: Convergence Trends for Turbulence Model

Figure 4.3 shows the convergence history of air of the turbulence model parameters in which RMS K-TurbKE is the root mean square for turbulence kinetic energy, and RMS O-TurbFreq is the root mean square for turbulence frequency. The solution of turbulence modeled equations was achieved after 400 iterations of the accumulated time step and a convergence criteria between $1.0e^{-}3$ and $1.0e^{-}4$.

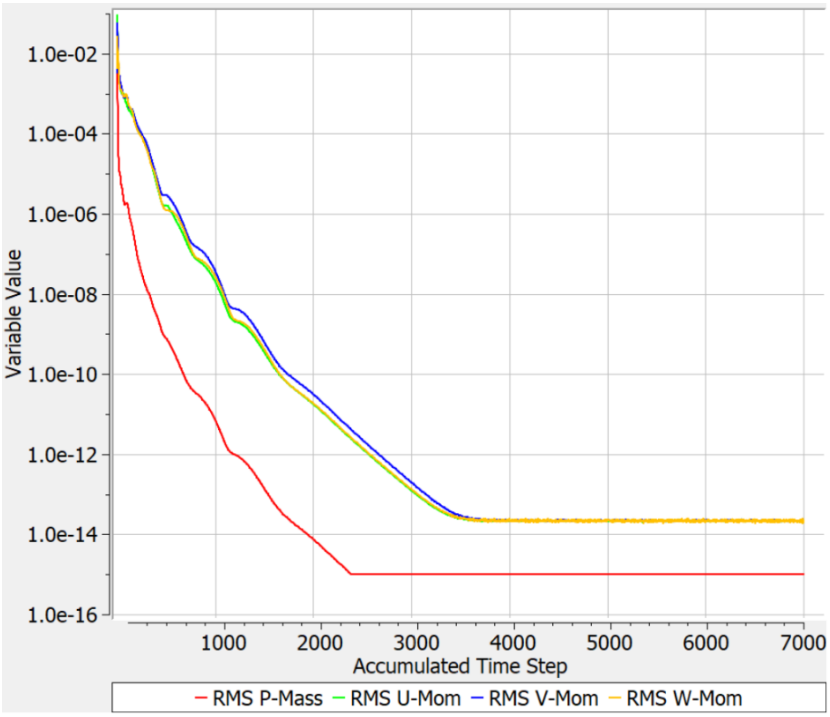

Figure 4.4: Convergence Trends for Mass and Momentum

Figure 4.4 shows the convergence criteria of syngas for mass and momentum. Syngas simulation took longer to converge than for air. This was attributed to the lower density of syngas compared to air. Convergence of the mass equation occurred after 2,500 iterations of the accumulated time step and at a value of $1.0e^{-}15$. The convergence of the momentum equation happened after 4,000 iterations at a value between $1.0e^{-}13$ and $1.0e^{-}14$.

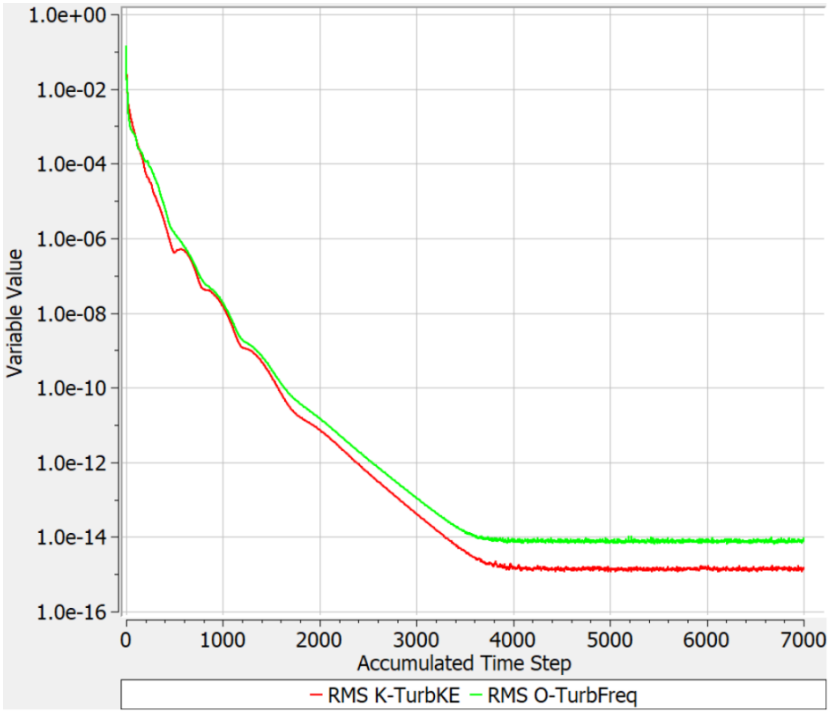

Figure 4.5: Convergence Trends for Turbulence Model

Shown in Figure 4.5 is the convergence history of turbulence modeled equations for syngas. Convergence of RANS equation for syngas occurred near the 4,800 iteration and at a convergence criteria of $1.0e^{-}14$.

4.4 VALIDATION OF SIMULATION

Validation of simulation of the compressor was studied by comparing the influence of fluid mass flow rate on pressure ratio at various compressor speeds as shown in Figure 4.6. The performance of the compressor was validated using air as the working fluid (Jiang, 2019).

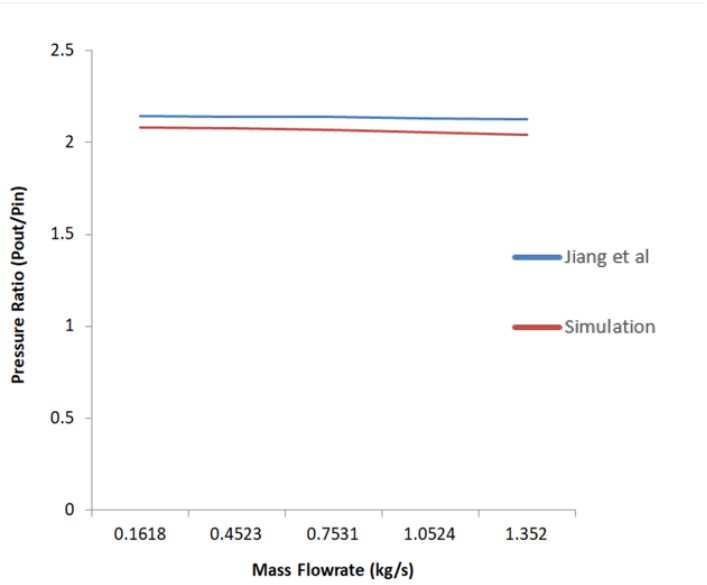

Figure 4.6: CFD Compressor Map Validation

From Figure 4.6 it was established that the level of agreement between simulation and experimental results was satisfactory with a difference of 1.03%.

4.5 PRESSURE DISTRIBUTION ACROSS THE CENTRIFUGAL COMPRESSOR

Figure 4.7 shows pressure distribution of air through the impeller at 22,000RPM and at a mass flowrate of 0.167kg/s. There was a 35.7% increase in pressure from the inlet to the outlet. The impeller increased the energy level of the fluid by whirling it outwards, thereby increasing the angular momentum of the fluid. Static pressure also increased within the impeller. As the fluid changed direction from axial to radial, the pressure reduced to -15,000Pa as highlighted in red in Figure 4.7. This reduction in pressure was attributed to secondary flow. The source of the secondary flow was the pressure gradient between the pressure side and the suction side of the blades brought about by centrifugal forces. Joslyn et al. (Joslyn, 1990) concluded that this low pressure region (shown in blue) was caused by centrifugal forces in the

boundary layers which drive the fluid from the hub to the shroud. Ang et al. (Wu, 2014) attributed this to vortex brought about by boundary layer interaction. Marco et al. (Lu, 2010) concluded that the flow separation on the impeller shroud was as a result of high curvature of the shroud.

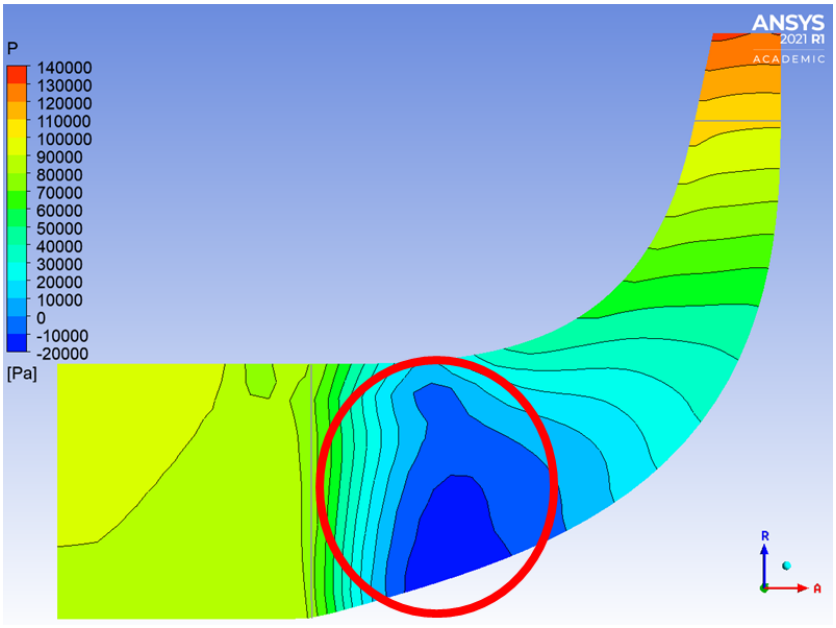

Figure 4.7: Air Pressure Contour at N=22000RPM

The observed pressure drop at the recirculation region is shown in Figure 4.8. Pressure values were obtained from the inlet to the outlet of the fluid domain and plotted in Figure 4.8. The values clearly showed the low pressure region occurs midway through the fluid domain. It was observed that the flow reversal brought about a decrease in pressure of air at the inlet. After the fluid changed direction, the pressure in the impeller region increased to 140,000Pa at the outlet. This behaviour was because of centrifugal forces in the compressor as observed by Joslyn et al. (Joslyn, 1990).

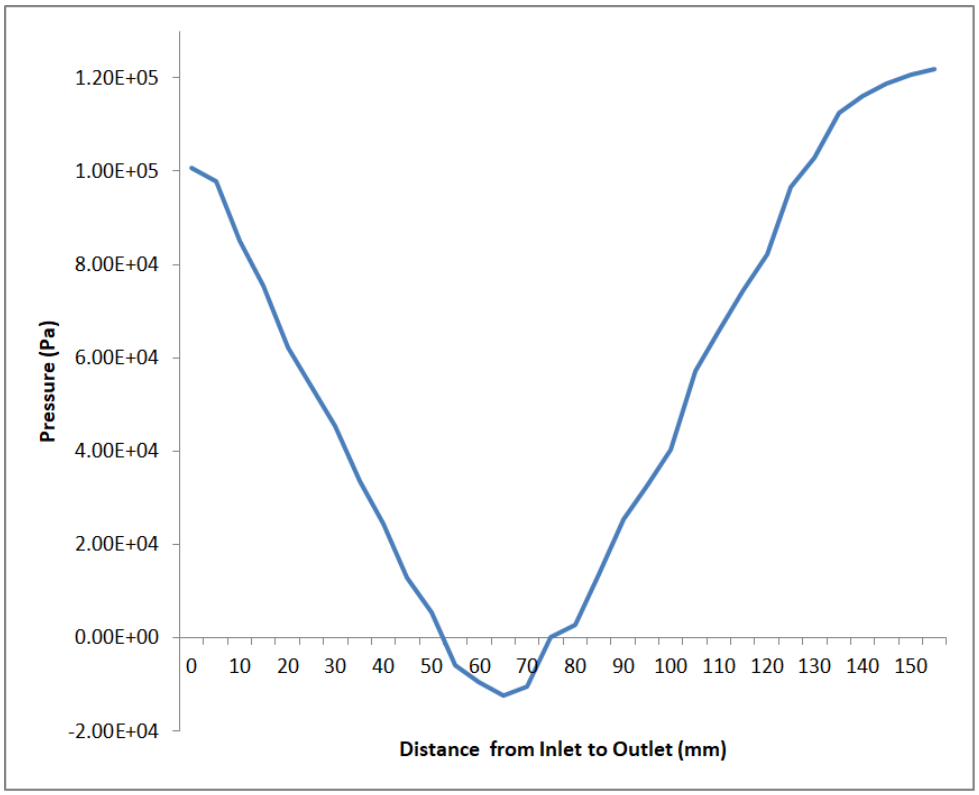

Figure 4.8: Pressure Distribution of Air at N=22000RPM

Figure 4.9 shows variation of the pressure distribution of air at different rotational speed from 18,000RPM to 22,000RPM. As the rotational speed increased, the separation region in the impeller also increased as seen in Figure 4.9. This was attributed to centrifugal forces and increase in incidence (angle). Incidence occurs when flow of the working fluid at inlet does not match with the inlet blade angle. Armin et al. (Joslyn, 1990) concluded that this was due to increase in blade loading attributed to higher blade speeds. There was a 40% increase in air pressure across the compressor.

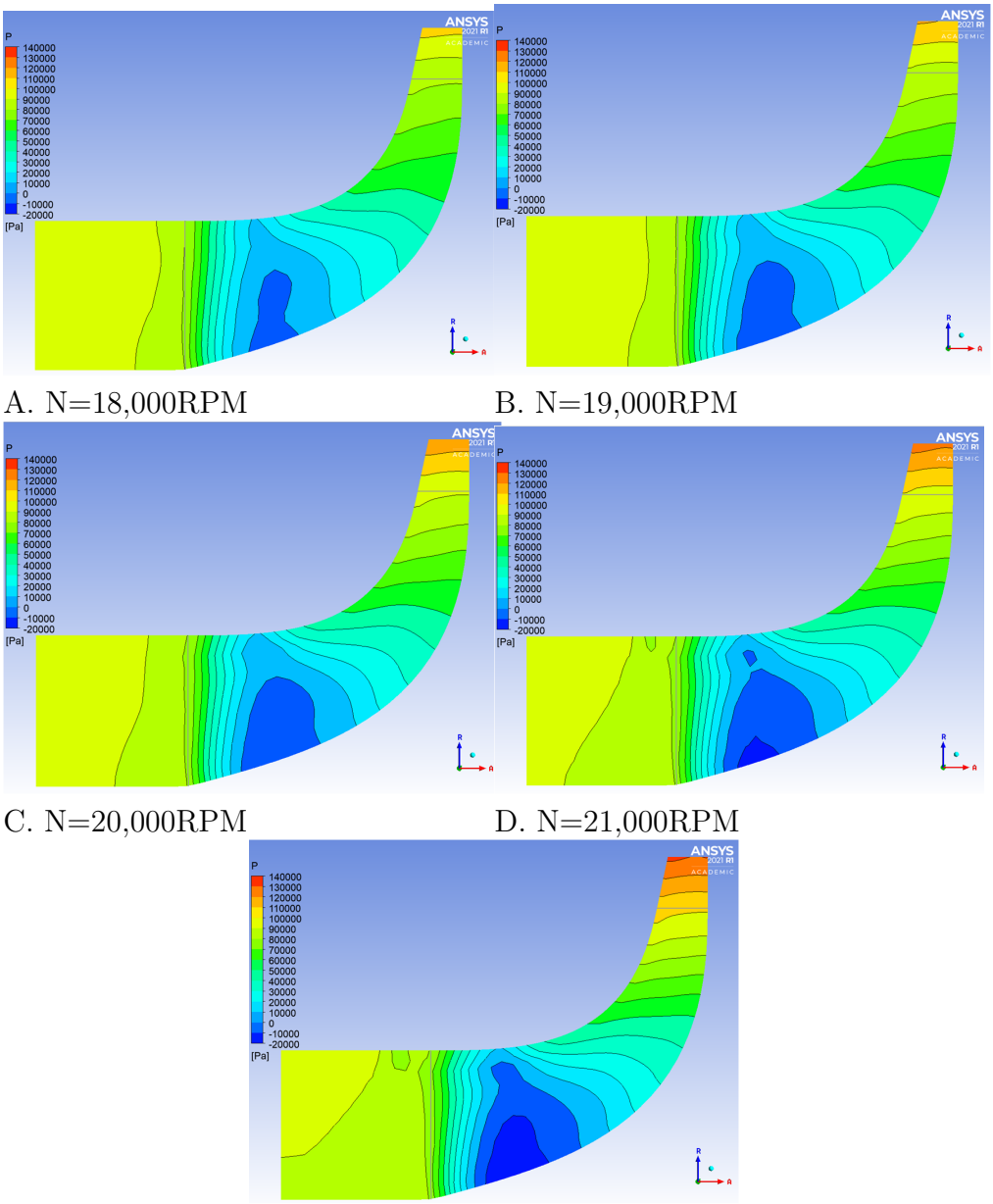

A. N=18,000RPM B. N=19,000RPM

C. N=20,000RPM D. N=21,000RPM

E. N=22,000RPM

Figure 4.9: Pressure Contours for Air at Varying Rotational Speed

Figure 4.10 shows the pressure distribution of syngas in the centrifugal compressor impeller. The pressure increased from the inlet but when the fluid changed direction from axial to radial, it reduced. The lowest pressures obtained was 97,000Pa and this

was attributed to secondary flow formation due to centrifugal force and incidence. Incidence occurs when flow of the working fluid at inlet does not match with the

inlet blade angle as discussed by Joslyn et al. (Joslyn, 1990). As seen in Figure 4.10 the highest pressure attained for syngas was 118,000Pa at the outlet while for air it was 140,000Pa. This is because syngas has a lower molecular weight of 7-10g/mol while of that of air is 28.9g/mol.

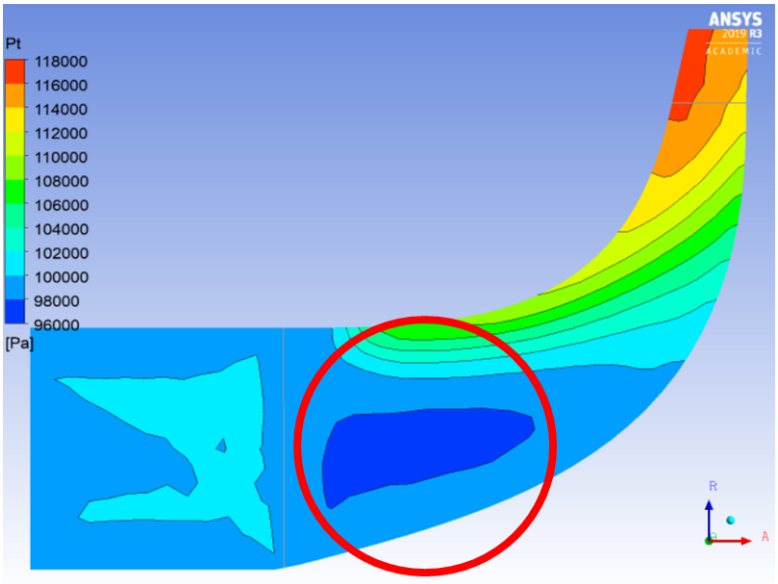

Figure 4.10: Pressure Contours at 22,000RPM

Figure 4.11 shows the pressure variations in syngas. It was noted that the recirculation region in syngas occured midway between the hub and shroud. For air, this region was on the suction side (it lay on the hub and extended towards the shroud). Joslyn et al. (Joslyn, 1990) observed this phenomenon and attributed it to centrifugal forces that created fluid flow from the hub towards the shroud. The pressure drop in air occurred from the inlet to 75mm from the inlet while for syngas, the pressure drop was from 8mm to 50mm. This difference is behaviour is mostly due to the molecular weight. With syngas being of lower molecular weight, the inlet pressures were not as affected by the recirculation region as that of air. There is scarce research indicating the distance of the recirculation region.

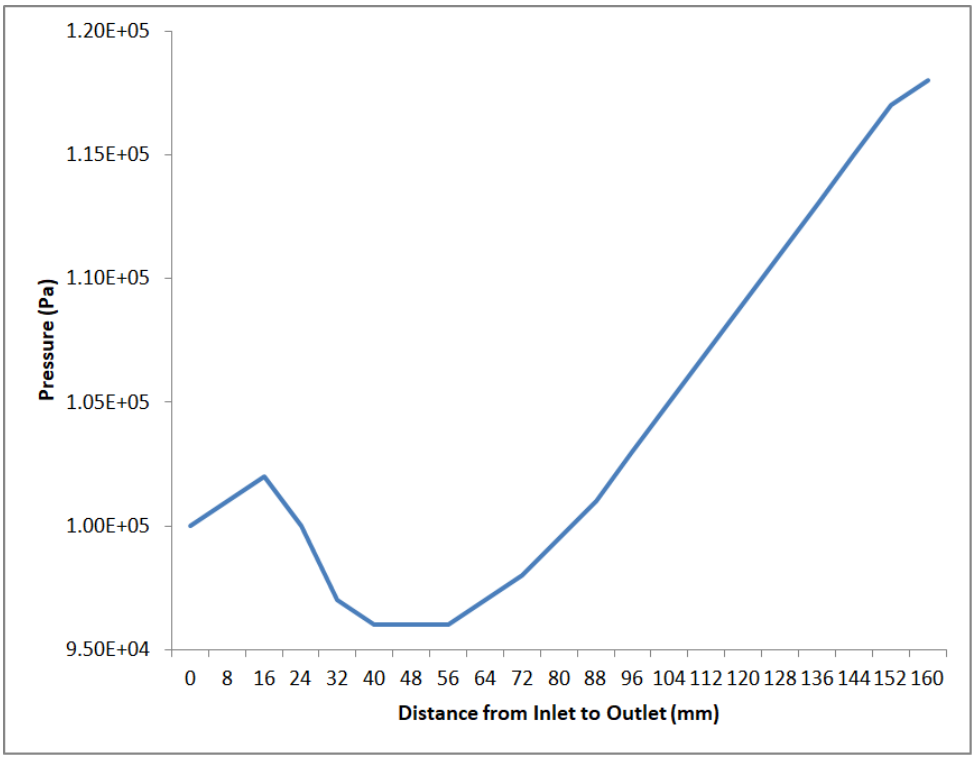

Figure 4.11: Pressure Distribution of Syngas at N=22000RPM

Figure 4.12 shows the pressure variations of syngas with increase in rotational speed from 18,000RPM to 22,000RPM. Syngas pressure increased by 17.24% from inlet to outlet. There were recirculation regions in the compressor attributed to centrifugal forces. With increase in rotational speed, the recirculation region reduced. The behaviour of air was different in that as the rotational speed increased, the recirculation region increased with the lowest region being at -20,000Pa. This behavioural difference was attributed to the molecular difference of both air and syngas.

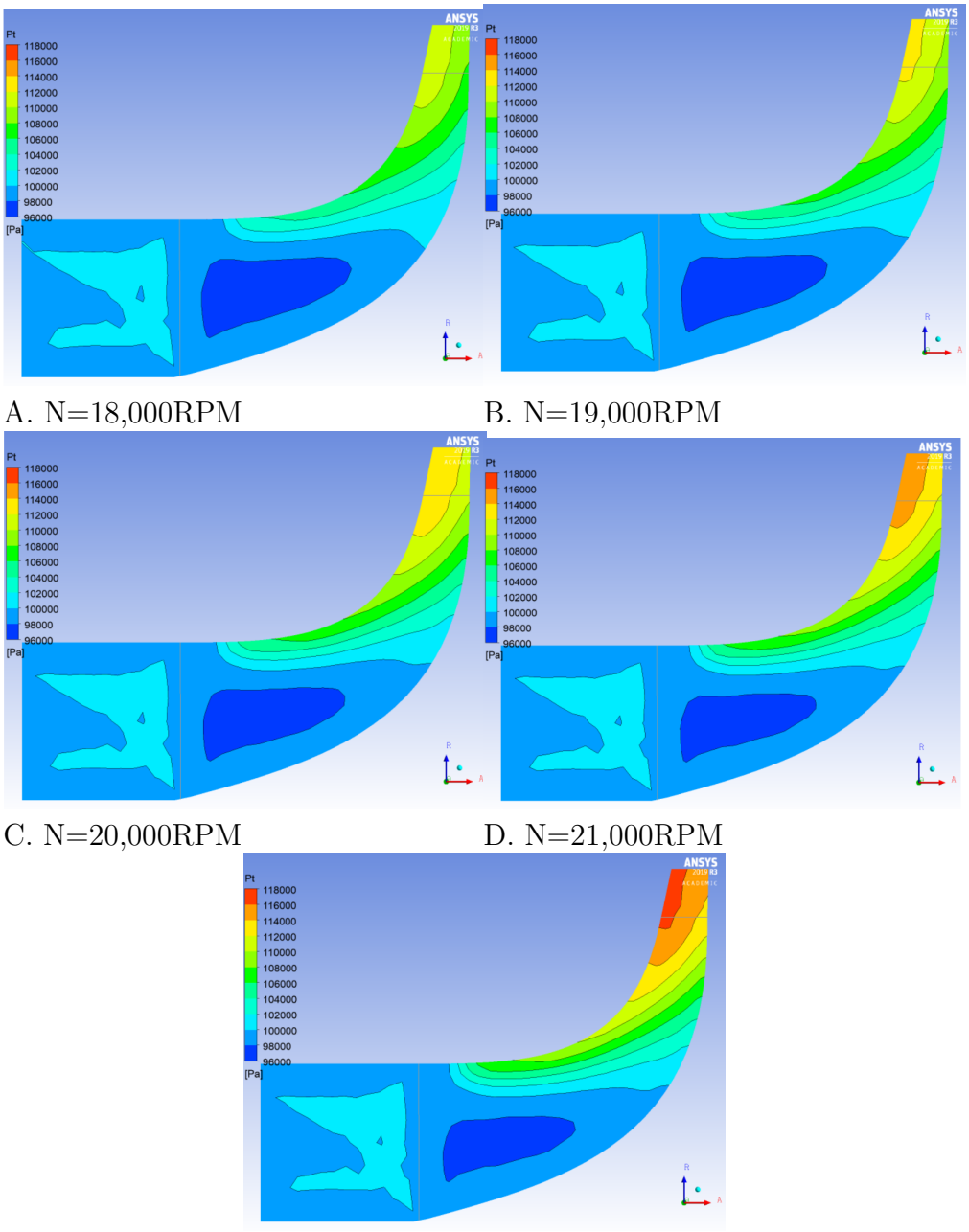

A. N=18,000RPM B. N=19,000RPM

C. N=20,000RPM D. N=21,000RPM

E. N=22,000RPM

Figure 4.12: Pressure Contours for Syngas at Varying Rotational Speed

Figure 4.13 shows comparison of pressure distribution between air and syngas. The low pressure region (shown as blue and circled in red) was more prominent in air than in syngas. One of the main reason for this is because air has a higher molecular weight than syngas. For air, the low pressure region originated from the hub towards the shroud while for syngas the low pressure region was midway between hub and

shroud. This showed that the centrifugal forces experienced as air was compressed was more than syngas. This information revealed that air experienced more stall than syngas and can be used in power gas turbines to determine the behaviour of the impeller blades over time.

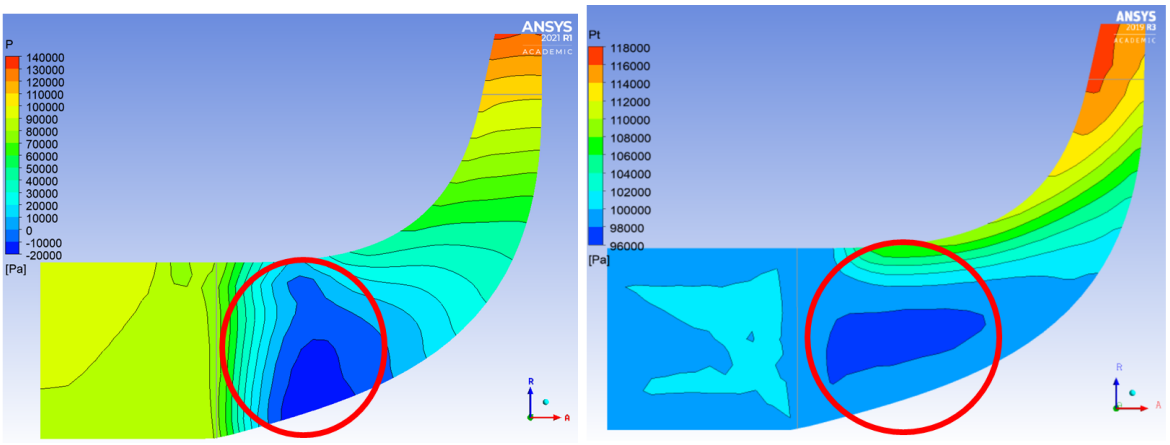

A. Air B. Syngas

Figure 4.13: Comparison of Pressure Contours between Air and Syngas

Figure 4.14 shows the pressure ratios of syngas and air. The highest pressure ratio attained by air was 1.2 while for syngas it was 0.95. The pressure ratios for syngas increased gradually while for air the increase was more significant. In their work Wang et al. (Wu, 2014) attained a pressure ratio of 1.17 and attributed this behaviour of increase in pressure ratio to the increase in rotational speed. With increase in rotational speed, the centrifugal forces increase and this also led to an increase in pressure ratio. Gas turbines in operation experience this and uses it to track onset of surge and choke.

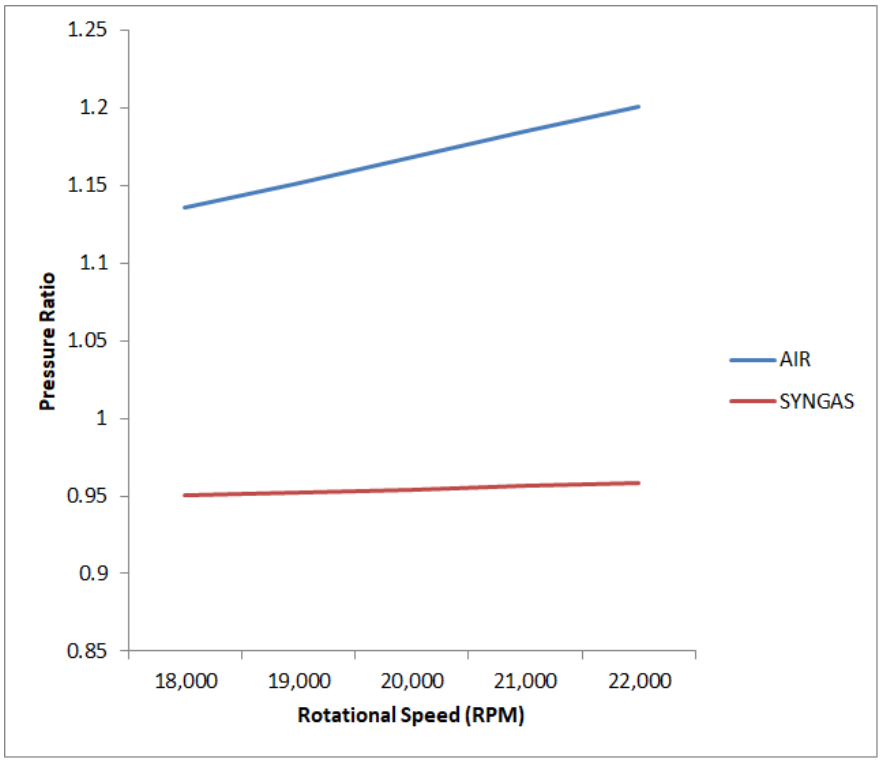

Figure 4.14: Pressure Ratio

4.6 FLOW THROUGH THE CENTRIFUGAL COMPRESSOR

The velocity of air through the compressor varied from shroud to hub. This was represented through span representation of velocity streamlines as shown in Figure 4.15. Span is the distance from hub to shroud (Joslyn, 1990).

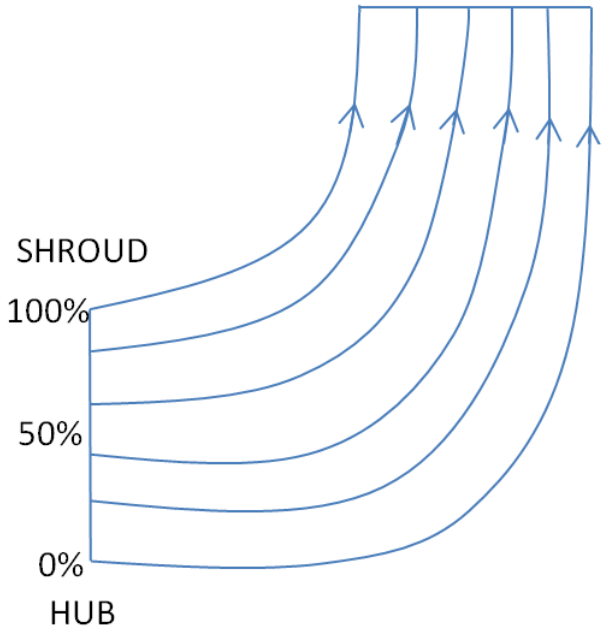

Figure 4.15: Velocity Streamlines in the Impeller

Figure 4.16 shows velocity changes at 20%, 50% and 80% span. A region of low velocity was observed originating from the leading edge on the pressure side of the impeller blades. Near the hub, the flow accelerated towards the impeller leading edge then decelerated. This deceleration was attributed to leading edge vortex formation as highlighted circled in red in Figure 4.16 A, B and C . Yang et al (Joslyn, 1990) observed this and concluded that the behaviour was brought about by centrifugal forces in the compressor. There were also regions of high velocity, of 160m/s, observed on the suction side of the impeller blades.

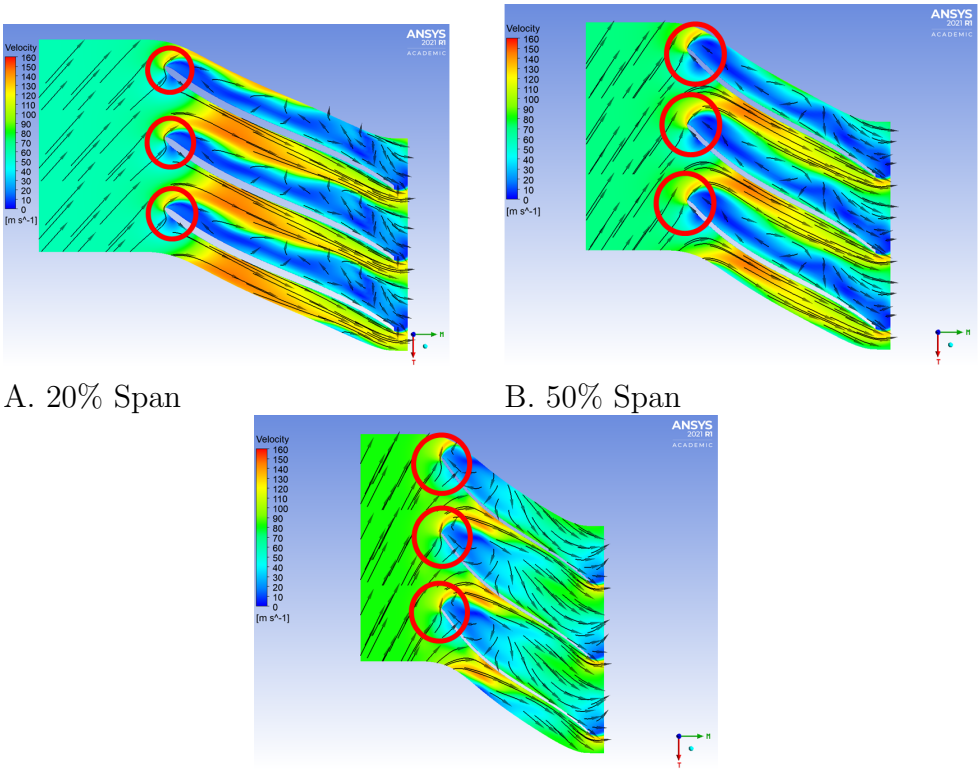

A. 20% Span

B. 50% Span

C. 80% Span

Figure 4.16: Velocity Distrbution for Air

As the rotational speed increased from 18,000RPM to 22,000RPM at 50% span, the change in velocity vector plots was a 55.56% increase as seen in Figure 4.17. Leading edge vortex was also observed at these rotational speeds as represented by the velocity vector plots.

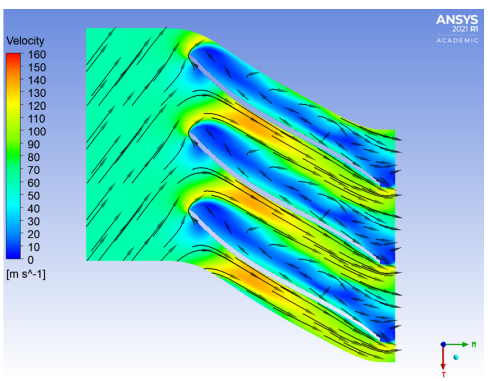

A. N=18,000RPM

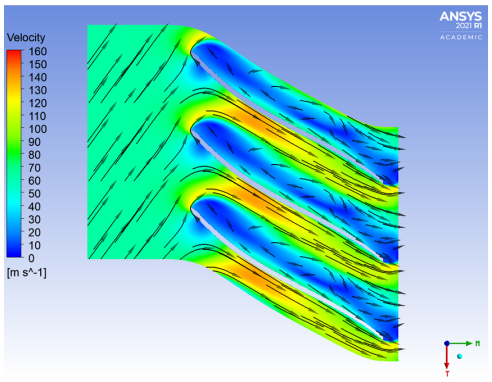

B. N=19,000RPM

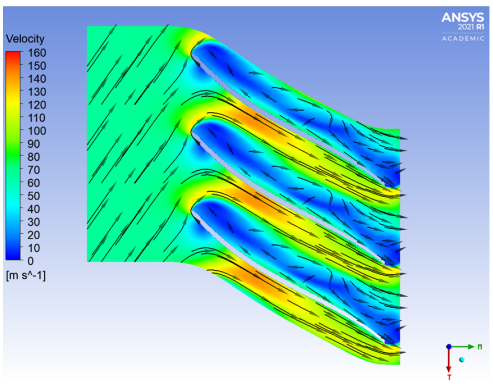

C. N=20,000RPM

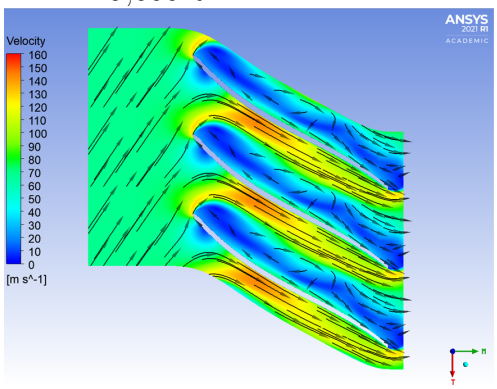

D. N=21,000RPM

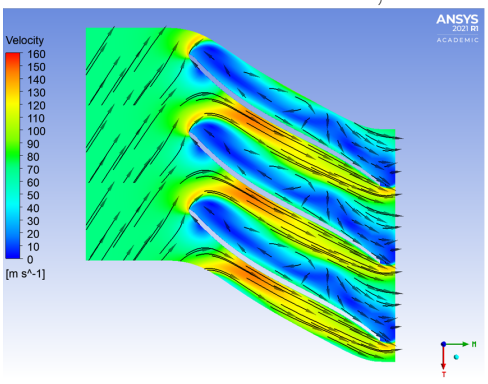

E. N=22,000RPM

Figure 4.17: Velocity Distribution at 50% Span for Air at Varying Rotational Speed

Figure 4.18 shows the velocity vector plots of syngas at a rotational speed of 22,000RPM. For syngas the region of recirculation was not as pronounced as observed in the analysis of pressure distribution in Section 4.5. There was however a low velocity region on the blade pressure side. It was also notable that the syngas flow rate was 500% higher than that of air with the maximum velocity attained being at the trailing

edge. There was minimal recirculation at 80% span. This behaviour of syngas was attributed to its low molecular weight coupled with low mass flowrate through the compressor at high speeds.

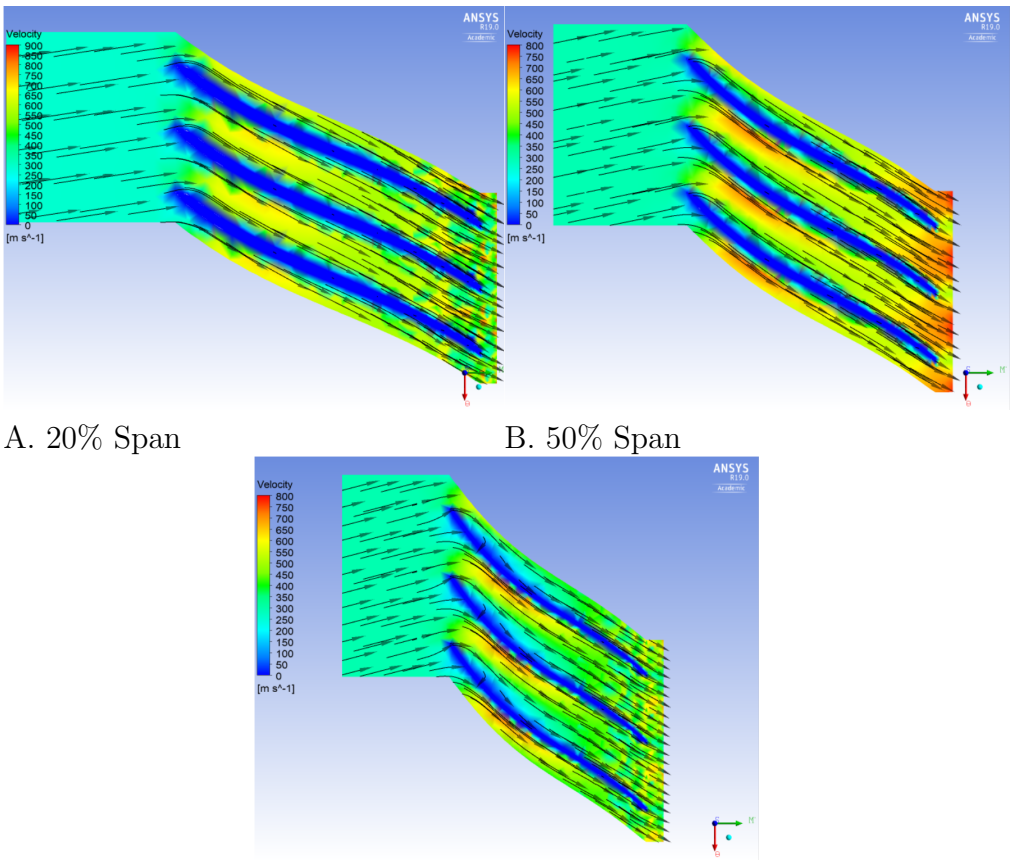

A. 20% Span B. 50% Span

C. 80% Span

Figure 4.18: Velocity Distribution for Syngas

With increase in rotational speed from 18,000RPM to 22,000RPM at 50% span there was an increase in the velocity downstream of the impeller blades by 62.5% as shown in Figure 4.19. Compared to air flow across the compressor, regions of high velocity notable for syngas account for the reduced pressure as observed in Section 4.5.

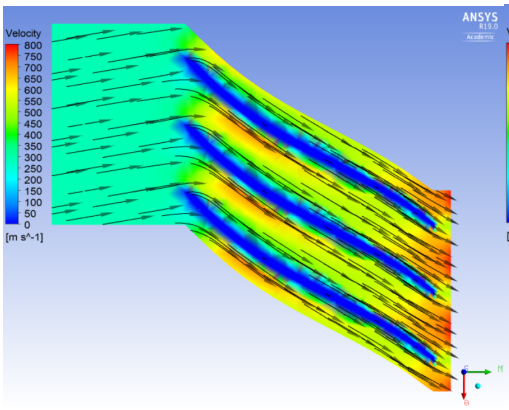

A. N=18,000RPM

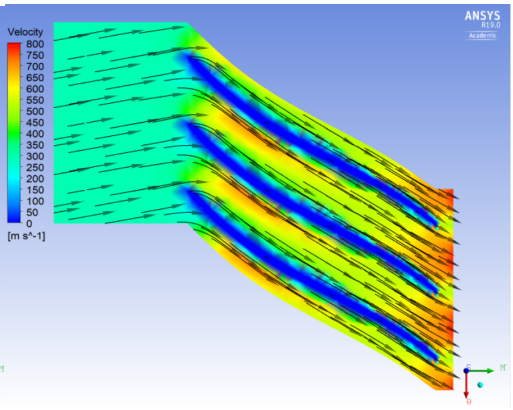

B. N=19,000RPM

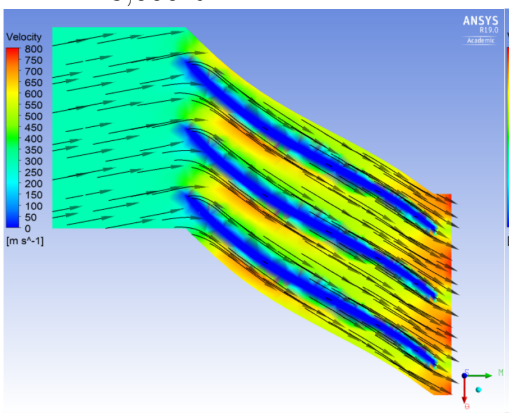

C. N=20,000RPM

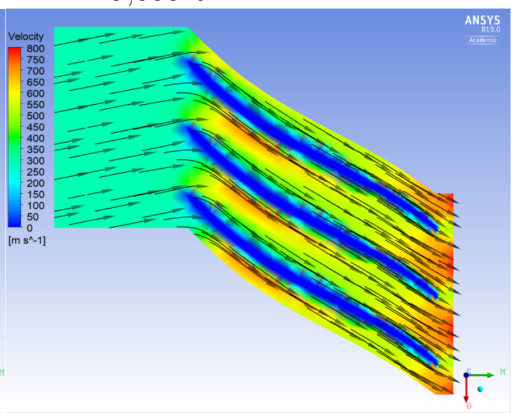

D. N=21,000RPM

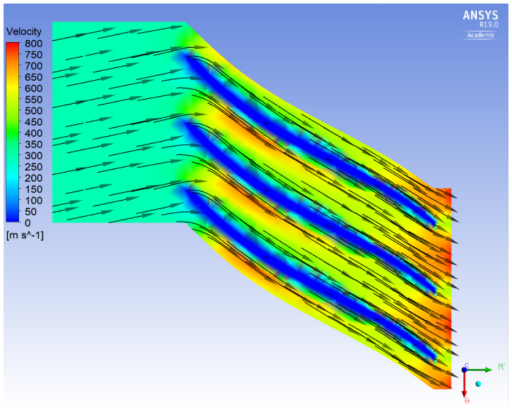

E. N=22,000RPM

Figure 4.19: Velocity Vectors at 50% Span for Syngas at Varying Rotational Speed

4.7 MACH NUMBER VARIATION ACROSS THE CENTRIFUGAL COMPRESSOR

Botha et al (Botha, 2012) described Mach number as a factor that influences compressor

efficiency and it is also used to reveal regions of formation of pressure waves in the compressor. Figure 4.20 shows changes in relative Mach number of air at rotational speeds of 18,000RPM to 22,000RPM. There was a steady rise in Mach number which was characterised by a region of high intensity at the suction side of the impeller blades. This was attributed to flow variations earlier observed at the recirculation region (observed in section 4.6).

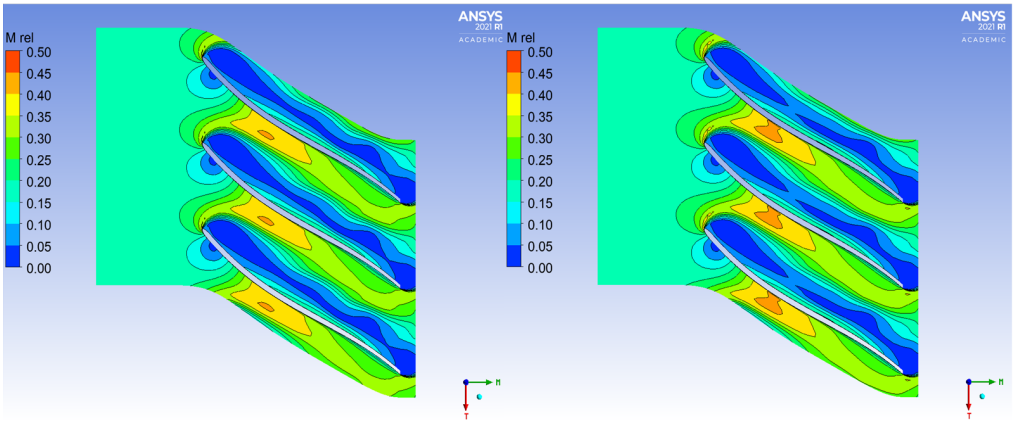

A. N=18,000RPM B. N=19,000RPM

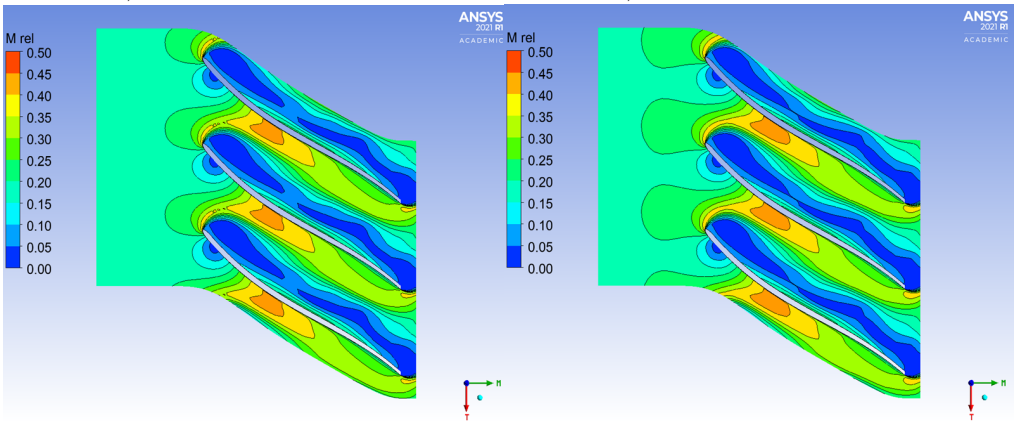

C. N=20,000RPM D. N=21,000RPM

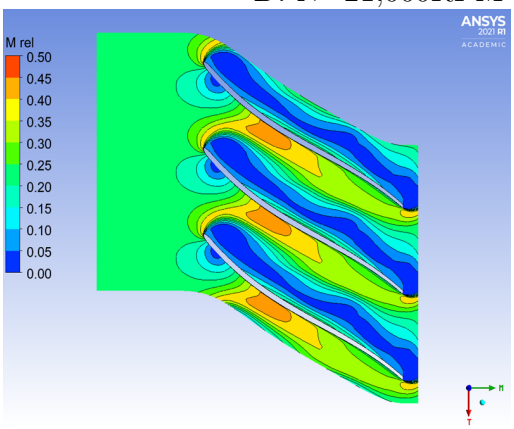

E. N=22,000RPM

Figure 4.20: Mach Number at 50% Span for Air at Varying Rotational Speed

Figure 4.21 shows the relative Mach number of syngas at 50% span. With increase in rotational speed, the relative Mach number increased particularly downstream at the exit region. This was attributed to the low molecular weight of syngas, regions

of high Mach number were observed at the outlet of the impeller.Mach number variation revealed the regions of formation of pressure waves.

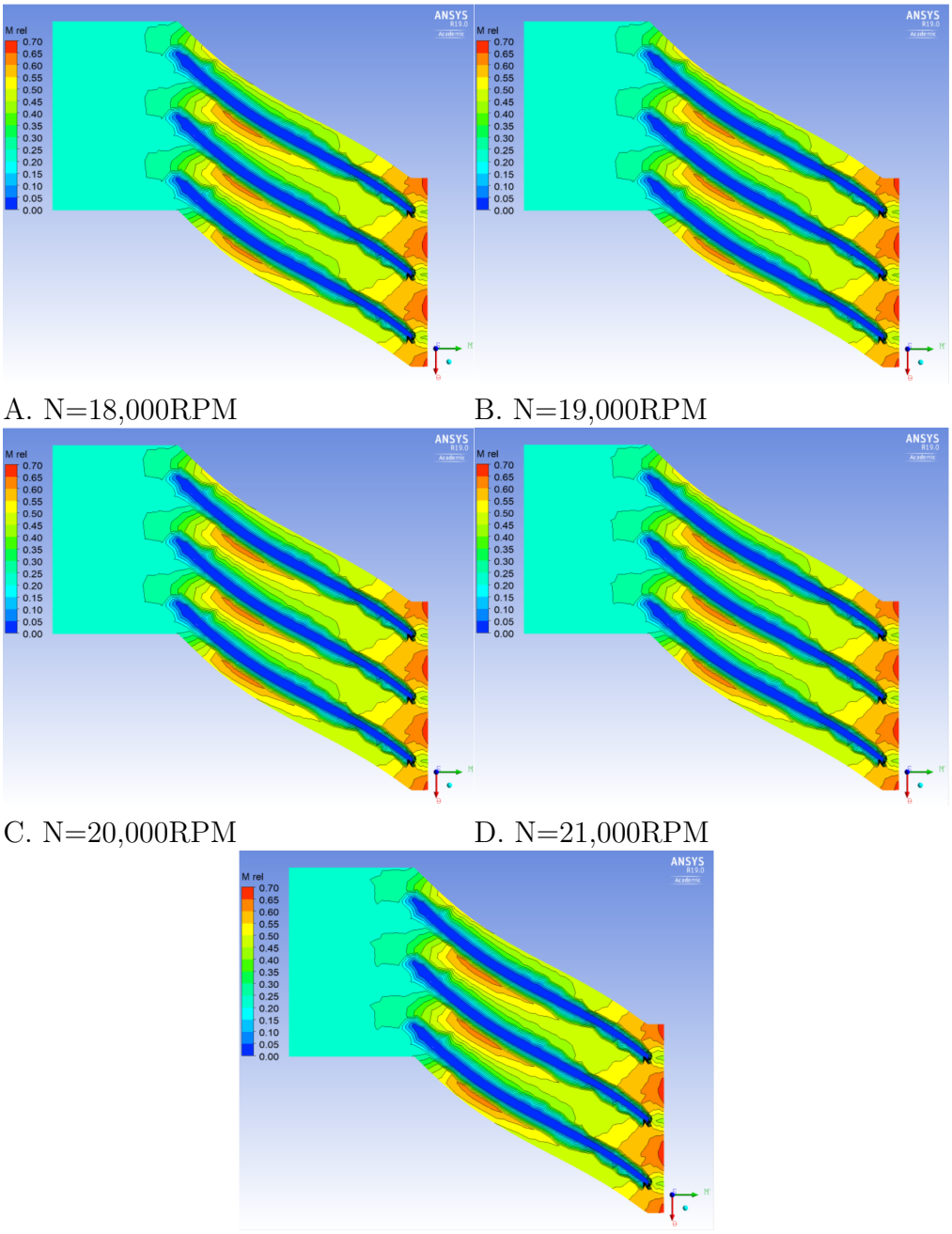

A. N=18,000RPM B. N=19,000RPM

C. N=20,000RPM D. N=21,000RPM

E. N=22,000RPM

Figure 4.21: Relative Mach Number at 50% Span for Syngas at Varying Rotational Speed

4.8 COMPRESSION EFFICIENCY

Figure 4.22 shows the compression efficiencies for air and syngas. The efficiencies increased to 85% for air and 67.5% for syngas, as the rotational speed increased at constant mass flow rate. This is because at constant mass flowrate with increase in speed, more power is available for the same work to be done therefore the efficiency increases. The maximum speed of 22,000RPM yielded the highest efficiency in the centrifugal compressor. Ang et al (Wu, 2014) attained an efficiency of 73% in his analysis of centrifugal compressor stage performance. The compression efficiency values were obtained directly from simulation output plots. Although the syngas efficiency was lower, the use of syngas has less emissions like NOx, CO and VOCs (Whitty, 2008). Syngas combustion produces 75% less CO_2 emmisions and 70% less GHG emissions as established by Xi et al (Lu, 2019).

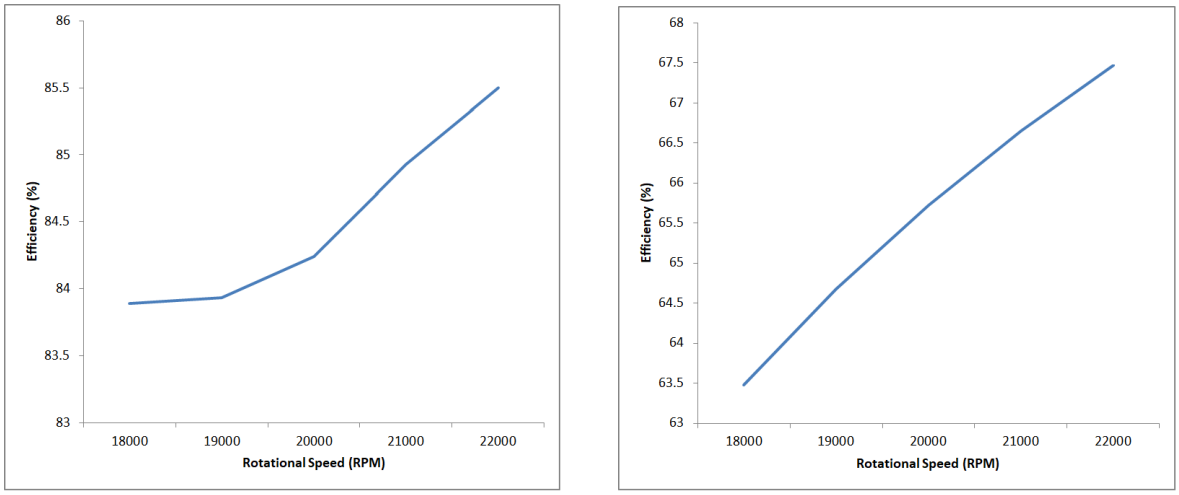

(a). Efficiency for Air (b). Efficiency for Syngas

Figure 4.22: Efficiency Graphs for Air and Syngas

CHAPTER FIVE

CONCLUSIONS AND RECOMMENDATIONS

5.1 CONCLUSION

In this research, a centrifugal compressor was designed and its flow investigated. The aim of the research was to investigate the use of syngas as an alternative source of energy in gas turbines. The performance of a compressor based on pressure and velocity distribution was studied and a number of conclusions were made as enumerated below.

1. There were centrifugal forces in the compressors which caused a region of low pressures as the flow changed direction from axial to radial. The low pressure regions were more pronounced for air than syngas. This difference was attributed to the low molecular weight of syngas as compared to air. Syngas has a molecular weight that is a quarter of that of air. These low pressure regions were on the
   suction side of the blades and were attributed to centrifugal forces in the compressor. The centrifugal forces push the fluid from the hub to the shroud. It was concluded that these centrifugal forces were higher in air than in syngas.

2. For velocity, there was leading edge vortex seen on the leading edge of the impeller blades. This region of low velocity was on the pressure side of the blades and it was attributed to secondary flows due to centrifugal forces. The velocity of syngas was 500% more than air attributed to low molecular weight of syngas which leads to higher velocity than air. These differences were seen in the velocity vector plots and Mach numbers. The velocity vector plots showed the recirculation region on the pressure side of the impeller blades. The conclusion was that the recirculation region was stall which occurs at the

impeller. There was a larger region of stall in air that in syngas due to the difference in molecular weight (Almasi, 2012).

3. Air flow through the compressor attained a higher efficiency than syngas. Though the compression efficiency of syngas obtained was lower than air, the benefits of using syngas is a 75% reduction in CO_2 and 70% reduction in GHG emission as compared to using coal directly as was established by Xi et al.(Lu, 2019). The
   conclusion drawn was that even though syngas compression yields lower efficiency, the reduction in emissions favours its use.

5.2 RECOMMENDATIONS

From this research and results and discussion the following recommendations are suggested:

1. It has been shown that the centrifugal compressor experienced centrifugal forces that brought about low pressure regions. The designed compressor had a sweep angle of 45^0. The behaviour of this sweep angle showed that backward swept blades affect rotor stage downstream (Neshat, 2015). This can be further investigated with
   compressor impeller blades at a different sweeping angles to determine the flow behaviour.

2. Coal syngas varies in composition depending on the coal used. For this study, the syngas had a ratio of 0.2 CO and 0.8 H_2. The behaviour of the syngas in the compressor showed regions of high velocity and high Mach numbers. The behaviour of coal syngas mixed with different ratios of biomass can be

simulated to study its behaviour in the compressor and determine how the addition of biomass affects the compressor performance.

3. For this study, the performance of an unshrouded impeller and vaneless diffuser were simulated. Unshrouded impeller was selected since it can attain higher tip speeds (Ludtke, 2004) while vaneless diffuser has no effect on compressor operation during flow instabilities (Kurz, 2011). Further studies can investigate the behaviour of syngas in shrouded compressors with vaneless diffusers to observe how reduced tip speeds affect compressor performance.

4. Low pressure region in the compressor was attributed to flow separation. Flow separation through the impeller shroud be further investigated to determine the exact position and to bring better understanding as to why it occurs. The boundary layers of air and syngas can be compared to further understand their behavior.

5. For this study, ANSYS student version was used. The student version has limitation in simulation. Future studies should be conducted using full version ANSYS to get more conclusive results.

REFERENCES

Ali, H. (2016). *Design of 8:1 pressure ratio centrifugal compressor* (Unpublished master's thesis). EDePro Company.

Almasi, A. (2012). Latest techniques and practical notes on antisurge systems for centrifugal compressors. *Australian Journal of Mechanical Engineering*, *10*, 81-90.

Banpurkar, R. (2015). Review paper on stress distribution over the blade of compressor of micro turbine. *International Journal of Advanced Engineering and Global Technology*, *3*, Issue 7.

Barma, S. D. (n.d.). *Ultrasonic-assisted cleaning of indian low-grade coal for clean and sustainable energy.* (2018, Journal of Cleaner Production)

Benini, E. (2003). Optimal navier stokes design of compressor impellers using evolutionary computation. *International Journal of Computational Fluid Dynamics*, *17*, 357-367.

Botha, B. (2012). *Design of a centrifugal compressor impeller for micro gas turbine application* (Unpublished doctoral dissertation). Stellenbosch University.

Boyce, M. P. (n.d.). Practical aspects of centrifugal compressor surge and surge control. In *Proceedings of the twelfth turbomachinery symposium.*

Bunyasi, M. M. (2012). Vulnerability of hydro-electric energy resources in kenya due to climate change effects: The case of the seven forks project. *Journal of Agriculture and Environmental Sciences*, 36-49.

Burnes, D. (2018). Performance degradation effects in modern industrial gas turbines. In *Proceedings of zurich 2018 global power and propulsion forum.*

Casleto, K. (2008). System issues and trade-offs associated with syngas production and combustion. *Combustion Science and Technology*, *180*, 1013-1052.

Chen, S. (2015). Coal gasification integration with solid oxide fuel cell and chemical looping combustion for high-efficiency power generation with inherent co_2 capture. *Elsevier: Applied Energy*, *146*, 298-312.

Council, W. E. (2013). *World energy resources survey* (Tech. Rep.).

Day, I. J. (2016). Stall, surge, and 75 years of research. *Journal of Turbomachinery, ASME*, *138*.

Emissions from coal fires and their impact on the environment (Tech. Rep.). (2009). US Geological Survey.

Filippisa, P. (2015). Biomass gasification plant and syngas clean-up system. *Science Direct: Energy Procedia*, *75*, 240-245.

Gibbons, T. (2007). *A review of materials for gas turbines firing syngas fuels* (Tech. Rep.). The Department of Energy.

International energy outlook may 2016 [Computer software manual]. (n.d.).

Jia, X. (2014). Study on internal flow and external performance of a semi-open impeller centrifugal pump with different tip clearances. *Research Gate*.

Jiang, H. (2019). Performance prediction of the centrifugal compressor based on a limited number of sample data. *Hindawi: Mathematical Problems in Engineering*.

Joslyn, D. (1990). Centrifugal compressor impeller aerodynamics (an experimental investigation). *The American Society of Mechanical Engineers*, *90-GT-128*.

Kengen's integrated annual report & financial statements for the year ended 30 june 2017.

.

Kenya national bureau of statistics: Statistical abstract 2015 [Computer software manual]. (n.d.).

Khadse, A. (2007). Underground coal gasification: A new clean coal utilization technique for india. *Elsevier Science Direct*, *32*, 2061-2071.

Kovalev, K. (2005). *Unstructured hexahedral non-conformal mesh generation* (Unpublished doctoral dissertation). Vrije Universiteit Brussel Belgium.

Kurz, R. (2011). Operation of centrifugal compressors in choke conditions. *Proceedings of the Fortieth Turbomachinery Symposium*, 129-136.

Li, S. (2014). Syngas spark ignition behavior at simulated gas turbine startup conditions. *Combustion Science and Technology*, *186*, 1005-1024.

Lu, X. (2010). Design and performance evaluation of a 10:1 pressure ratio centrifugal compressor impeller. *Proceedings of the ASME 2010 International Mechanical Engineering Congress and Exposition*.

Lu, X. (2019). Gasification of coal and biomass as a net carbon negative power source for environment-friendly electricity generation in china. *PNAS*.

Ludtke, K. H. (2004). *Process centrifugal compressors*. Springer-Verlag Berlin Heidelberg.

Mavriplis, J. (1997). Unstructured grid techniques. *Annual Reviews Fluid Mechanics*, *29*, 473-514.

Mostafa, N. (2006). Prediction of surge and rotating stall in compressor. *Proceedings of ICFDP: 8th International Congress of Fluid Dynamics and Propulsion*.

Nagpurwala, P. Q. (n.d.). *Centrifugal compressors* (Tech. Rep.). M.S. Ramaiah School of Advanced Studies.

Neshat, M. (2015). Investigating the effect of blade sweep and lean in one stage of an industrial gas turbine's transonic compressor. *Propulsion and Power Research, Elsevier*, *44*, 221-229.

Noman, S. (2006). The influence of tip clearance on centrifugal compressor stage of a turbocharger. In *Proceedings of the 4th wseas international conference on fluid mechanics and aerodynamics, elounda, greece.*

Nucara, P. (2013). *Design of gas turbine axial compressor for fuel flexibility* (Unpublished doctoral dissertation). University of Sussex.

Oyedepo, S. (2014). Thermodynamic analysis of a gas turbine power plant modeled with an evaporative cooler. *International Journal of Thermodynamics (IJoT)*, *17*, 14-20.

Peirs, J. (2004). A micro gas turbine unit for electric power generation: Design and testing of turbine and compressor. In *9th international conference on new*

actuators.

Rodgers, C. (2000). Effects of blade number on the efficiency of centrifugal compressor impellers. *ASME Turbo Expo*.

Rubanova, A. (n.d.). *History of compressors* (Tech. Rep.). Lund University.

Schleer1, M. (2008). Clearance effects on the onset of instability in a centrifugal compressor. *Journal of Turbomachinery*, *130*.

Semlitsch, B. (2016). Flow phenomena leading to surge in a centrifugal compressor. *Elsevier*, *103*, 572-587.

Shehadeh, M. (2017). Design of a single stage centrifugal compressor as part of a microturbine running at 60000 rpm: Developing a maximum of 60 kw electrical power output. *American Journal of Aerospace Engineering*, *4*, 6-21.

Spittle, P. (2003). *Gas turbine technology* (Tech. Rep.). Rolls-Royce.

Srinivas, G. (2014). Numerical simulation of centrifugal compressor. *ARPN Journal of Engineering and Applied Sciences*, *9*.

Trbinjac, I. (2015). Full-annulus simulation of the surge inception in a transonic centrifugal compressor. *Journal of Thermal Science*, *24*.

Usaid kenya: Power africa fact sheet. (n.d.).

Wang, T. (2012). Numerical study on a high-pressure stage in synthesis gas compressor. *Journal of Thermal Science and Technology*.

Whitty, K. (2008). Emissions from syngas combustion. *Combustion Science and Technology*.

Wu, Y. A. (2014). Numerical investigation of the performance and flow behaviour of centrifugal compressor. *Master's Thesis: University of Manchester*.

Xinqian, Z. (2015). Experimental investigation of surge and stall in a high-speed centrifugal compressor. *Journal of Propulsion and Power*, *31*.

Xu, X. (2017). Clean coal technologies in china based on methanol platform. *Elsevire Science Direct*.

Zemp, A. (2006/2007). *Cfd investigation on inlet flow distortion in a centrifugal*

compressor (Unpublished master's thesis). Swiss Federal Institute of Technology, ETH, Zurich Turbomachinery Laboratory.

Zhang, D. (2014). Tackling air pollution in china: What do we learn from the great smog of 1950s in london. *Sustainability*, *ISSN 2071-1050*.

Zikanov, O. (2010). *Essential computational fluid dynamics*. John Wiley & Sons, Inc.